

# Subclonal reconstruction of tumors using machine learning and population genetics

Giulio Caravagna<sup>1</sup>, Timon Heide<sup>1</sup>, Marc J. Williams<sup>2</sup>, Luis Zapata<sup>1</sup>, Daniel Nichol<sup>1</sup>, Ketevan Chkhaidze<sup>1</sup>, William Cross<sup>2</sup>, George D. Cresswell<sup>1</sup>, Benjamin Werner<sup>1</sup>, Ahmet Acar<sup>1</sup>, Louis Chesler<sup>3</sup>, Chris P. Barnes<sup>4</sup>, Guido Sanguinetti<sup>5,6</sup>, Trevor A. Graham<sup>2,§</sup>, Andrea Sottoriva<sup>1,§</sup>.

<sup>1</sup>Evolutionary Genomics and Modelling Lab, Centre for Evolution and Cancer, The Institute of Cancer Research, London SM2 5NG, UK.

<sup>2</sup>Evolution and Cancer Lab, Barts Cancer Institute, School of Medicine and Dentistry, Queen Mary University of London, London EC1M 6BQ, UK.

<sup>3</sup>Division of Clinical Studies, The Institute of Cancer Research, London SM2 5NG, UK.

<sup>4</sup>Department of Cell and Developmental Biology and UCL Genetics Institute, University College London, London WC1E 6BTCL, UK.

<sup>5</sup>School of Informatics, University of Edinburgh, Edinburgh, EH8 9AB.

<sup>6</sup>International School for Advanced Studies - SISSA, Via Bonomea 265, Trieste 34136, IT.

§correspondence to Trevor A. Graham ([t.graham@qmul.ac.uk](mailto:t.graham@qmul.ac.uk)) and Andrea Sottoriva ([andrea.sottoriva@icr.ac.uk](mailto:andrea.sottoriva@icr.ac.uk)).

## Abstract

The majority of cancer genomic data are generated from bulk samples composed of mixtures of cancer subpopulations, as well as normal cells. Subclonal reconstruction approaches based on machine learning aim to separate those subpopulations in a sample and reconstruct their evolutionary history. However, current approaches are entirely data-driven and agnostic to evolutionary theory. We demonstrate that systematic errors occur in the analysis if evolution is not accounted for, and this is exacerbated by multi-sampling of the same tumor. We present a novel approach for model-based tumor subclonal reconstruction (MOBSTER) that combines machine learning with theoretical population genetics. Using public whole-genome sequencing data from 2,606 samples from different cohorts, new data and synthetic validation, we show this method is more robust and accurate than current techniques in single sample, multi-region and longitudinal data. This approach minimizes the confounding factors of non-evolutionary methods, leading to more accurate recovery of the evolutionary history of human cancers.

## Introduction

Cancers change over time through a process of clonal evolution<sup>1</sup>, inevitably resulting in intra-tumor heterogeneity<sup>2</sup>. Genome sequencing of one or more bulk samples from tumors has become the most common way to study clonal evolution in human malignancies, and studies are dedicated to the identification of cancer (sub)clones<sup>3</sup>. A cancer “clone” remains a loosely defined entity, and its purest definition is “a group of cells within the tumor that share a common ancestor”. In phylogenetic terms, this would represent a monophyletic clade. However, this implies that any ancestor in the entire phylogenetic tree of a tumor can be identified as the founder of a distinct “clone”, even though it may show no biological difference from the rest of the cancer cells. This is why in the field we implicitly identify clones “of interest”, such as those that have growth/survival advantage (an ancestor under positive selection), or those that generate metastases (an ancestor that arrived and grew at a given metastatic site). The limits in the definition of a clone are important to bear in mind when attempting to recover the tumor clonal architecture.

To identify clones in bulk cancer samples, the established approach is unsupervised clustering of variant read counts<sup>4</sup>, with each of the resulting clusters defined as a clone. This procedure, called “subclonal reconstruction”, leverages on variant read counts and associated variant allele frequency (VAF) of somatic mutations, adjusted for copy number status and tumor purity, to identify groups of variants with similar cellular proportions. Subclonal reconstruction allows tracing the “life history” of a tumor via determination of its phylogenetic tree (sometimes called a “clone tree”)<sup>3</sup>.

Current methodologies approach subclonal reconstruction with sophisticated mixture models<sup>4</sup>, implemented via Dirichlet Processes<sup>3,5,6</sup> or Dirichlet finite mixtures<sup>7</sup>. These machine learning methods are entirely data-driven and are usually chosen because of their convenient statistical properties, rather than their adherence to the mechanisms of tumor evolution. They can be efficient and accurate, as long as the underlying assumptions are

56 correct. All current subclonal reconstruction methods assume that variant read counts from bulk tumor samples  
57 present as a mixture of Binomial or Beta-Binomial mutational clusters, each one corresponding to a clone.  
58 However, these are not the only observable patterns in the data: the mutations that occur within each clone while  
59 it expands are also detectable. Given the size of the human genome, even with low mutations rates (e.g.  $10^{-9}$   
60 nucleotide substitutions per base per division<sup>8</sup>), new mutations are expected at each cell division, and thus large  
61 numbers of passenger mutations inevitably accumulate within an expanding clone. The evolutionary dynamics  
62 of this passenger mutation accumulation are *neutral*, and give rise to a power-law distributed “tail” of ever more  
63 mutations at ever lower frequency. This has been mathematically demonstrated in theoretical population  
64 genetics<sup>9-14</sup> and is corroborated by genomic data at high resolution<sup>15,16</sup>. These within-clone neutral tails have not  
65 been directly addressed by previous methods, potentially confounding the measurement of clonal heterogeneity.

66  
67 Here, we reconciled data-driven machine learning approaches to clustering VAFs and corresponding Cancer  
68 Cell Fractions (CCF), with the insight given by evolutionary theory. Specifically, we combined Dirichlet  
69 mixture models with the distributions predicted by theoretical population genetics models<sup>9-12</sup>, producing a  
70 model-based method for subclonal reconstruction called MOBSTER (MOdel Based cluSTering in cancER).  
71 MOBSTER can process mutant allelic frequencies to identify and remove neutral tails from the input data, so  
72 that machine-learning subclonal reconstruction algorithms can be applied downstream to find subclones from  
73 read counts. We also expanded MOBSTER to analyze data from multiple samples of the same tumor, collected  
74 both in space and time.

## 75 Results

### 76 77 Mutation, drift and selection

78  
79 Cancers grow from a single cell, and hence neutral mutations that occur in the first few cell divisions are present  
80 at high frequency in the final population, irrespective of the action of selection. In addition, stochastic  
81 fluctuations in population size of cell lineages can also increase the frequency of mutations in the absence of  
82 selection; this is called genetic drift<sup>17</sup>. The same is true within (sub)clones: a clone originates as a single cell,  
83 and neutral mutations that occur early within the clone are found in a large proportion of the clone’s cells.  
84 Fundamental insight into the accumulation of mutations in the absence of positive selection came from the study  
85 of the Luria-Delbruck model in bacteria<sup>18</sup>. This has led to well-established population genetics theory describing  
86 the accumulation of mutations within neutrally growing populations<sup>10,11</sup>. The same theory applies to cancer  
87 clones<sup>9,12</sup> and can be extended to include positive selection<sup>16</sup>. Theory states that we should expect a tail of  
88 neutral passenger mutations within a clone (Figure 1a). Neutral tails only recently became evident in cancer data  
89 with the adoption of high-depth whole genome sequencing (WGS), as lower depth sequencing (e.g. <60x) is  
90 insufficient to detect tails reliably<sup>16</sup>, and exome or panel sequencing often assay too few mutations to show a  
91 clear VAF spectrum.

92  
93 Figure 1a shows the simplest example of a uniform ‘neutral’ tumor expansion. The corresponding clone tree has  
94 a single “truncal” node (Figure 1b). The VAF spectrum for this tumor consists of a “clonal peak” at high  
95 frequency, corresponding to the mutations that are present in all cells (i.e. in the most recent common ancestor,  
96 MRCA), and a neutral tail of mutations at lower VAF generated as the clone expands (Figure 1c). In the case  
97 where a subclone with selective advantage is present (Figure 1d,e), the data will present as two peaks at high  
98 frequency (one clonal and one subclonal) as well as a mixture of two overlapping neutral tails<sup>16</sup> (Figure 1f).  
99 Performing subclonal reconstruction on these data assuming a generative mixture of just Binomial or Beta-  
100 Binomial distributions will detect several clusters within the neutral tail that are erroneously identified as  
101 subclones, as illustrated in two simulated cases (neutral in Figure 1g, and with one selected subclone in Figure  
102 1h). Importantly, mutations in neutral tails are not monophyletic, and hence grouping them together into clones  
103 is erroneous even under the strictest definition of a clone. Moreover, when these incorrect clones are used  
104 downstream for phylogenetic reconstruction, the resulting trees (Figure 1i) have a very different structure from  
105 the true trees (Figure 1b,e), thus propagating errors and uncertainty in the tree construction, with many  
106 equivalent (but wrong) trees potentially fitting the same data.

107  
108 Moreover, low-depth sequencing and low purity data cause neutral tails to be under-sampled and likely to be  
109 mistaken for subclones, as they lose their characteristic power-law shape. Simulated WGS data (Figure 1j) show  
110 that with low coverage or purity, the signal of a neutral tail becomes statistically difficult to distinguish from  
111 that of a selected subclonal cluster (Figure 1k). This observation indicates that sequencing depth below  
112 90x/100x and low purity prevents reliable subclonal reconstruction. We note that patterns of noisy subclonal

113 VAF distributions that may represent under-sampled tails (e.g. Figure 1k), are commonly observed in cancer  
114 sequencing data at depth  $<90\times/100\times$ .  
115

## 116 Model-based clustering of variant allelic frequencies

117  
118 The frequency  $f$  of newly acquired passenger mutations in an expanding population follows a Landau  
119 distribution<sup>10</sup>, which at the frequency range detected by current sequencing standards can be approximated by a  
120 power law distribution  $X \sim 1/f^2$  (Figure 2a), as we previously reported<sup>9</sup>. Subclonal alleles under positive  
121 selection, together with their hitchhiking passengers, will instead form clusters in the VAF distribution as they  
122 rise in frequency due to positive selection<sup>16,19</sup>.  
123

124 We can model VAFs or fraction data via Beta distributions<sup>7</sup>, and model read counts with Binomial or Beta-  
125 Binomial distributions<sup>3,5-7</sup>. In MOBSTER (Figure 2a), we model the evolutionary dynamics of a growing tumor  
126 containing subclones by combining Beta distributions (expected from subclones under selection) with a power  
127 law (expected from neutral tails). After fitting the VAF distribution, tail mutations can be removed and  
128 clustering of read counts from the remaining mutations can be performed via standard methods (Figure 2b).  
129 MOBSTER controls for tails while retaining the original variance of the data when clustering non-tail read  
130 counts downstream. Notably, MOBSTER always compares the fit of a mixture of clones with and without a  
131 neutral tail and uses a regularized model selection strategy to determine the best model fit to the data.  
132

133 MOBSTER combines one Pareto Type-I random variable (a type of power-law) with  $k$  Beta random variables,  
134 resulting in a univariate finite mixture with  $k + 1$  components. The likelihood for  $n$  datapoints  $x_i$  is  
135

$$p(D|\theta, \pi) = \prod_{i=1}^n \left[ \pi_1 g(x_i|x_*, \alpha) + \sum_{w=2}^k \pi_w h(x_i|a_{w-1}, b_{w-1}) \right],$$

136  
137 where  $g$  and  $h$  are density functions,  $\theta = (x_*, \alpha, a_1, \dots, a_k, b_1, \dots, b_k)$  is a vector of parameters and  $\pi$  are mixing  
138 proportions in a standard setting with  $n \times (k + 1)$  latent variables. The Pareto component follows  $g(x|x_*, \alpha) \propto$   
139  $1/x^{1+\alpha}$  for  $x \geq x_*$ , and the Beta follows  $h(x|a, b) \propto x^{a-1}(1-x)^{b-1}$  in  $[0,1]$ . A derivation of MOBSTER, its  
140 relation to other approaches and technical comments are available in the Online Methods.  
141

142 In the hypothetical example of a “functionally monoclonal” tumor with neutral subclonal dynamics (Figure 1a),  
143 MOBSTER fits  $k = 1$  Beta clusters of truncal mutations (present in all cancer cells) plus a neutral tail (Figure  
144 2c). Similarly, for a tumor with one selected subclone (Figure 1d), MOBSTER fits  $k = 2$  Beta clusters and a tail  
145 (Figure 2d). When we identify and remove tail mutations from the data, subsequent clustering of read counts  
146 mutations identifies the true tumor clones and their correct clone trees (inner clone tree panels).  
147

## 148 Synthetic validation of the method and confounding factors

149  
150 We used synthetic data to validate MOBSTER and quantify the degree to which neutral tails confound subclonal  
151 deconvolution with standard methods (Supplementary Note, Supplementary Figures 1-9). We used a stochastic  
152 branching process<sup>16</sup> to simulate the growth of  $n = 150$  tumors (Online Methods and Supplementary Data  
153 vignette “Example Subclonal Dynamics”). Out of these 150 cases, 30 tumors were neutral (as Figure 1a) and  
154 120 contained one selected subclone (as Figure 1d). For each tumor we simulated bulk WGS at 120x median  
155 coverage and 100% purity. In every test, we always compared the fit of MOBSTER with and without a tail,  
156 retaining the best; we then recorded the predicted number of selected clones,  $k$ , and the fit precision  
157 (Supplementary Figure 3 and 4). We note that by applying further population genetics theory<sup>16</sup> to the output of  
158 MOBSTER, we can estimate the tumor evolutionary parameters, such as the mutation rate, the time of  
159 emergence of subclones, and their selection coefficients (Supplementary Figure 5). We also carried out several  
160 other tests for the detection of low-frequency subclones admixed with tails (Supplementary Figures 6 and 7).  
161

162 By accounting for neutral tails, MOBSTER significantly outperformed standard approaches based on both  
163 Dirichlet variational mixtures and Dirichlet Processes (Extended Data Figure 1), two statistical frameworks at  
164 the core of subclonal reconstruction tools like sciClone<sup>7</sup>, pyClone<sup>5</sup>, DPclust<sup>3</sup> and many others. Results are  
165 consistent for various parameterizations, in particular of the concentration parameter  $\alpha > 0$ , which determines  
166 the propensity of adding clusters to the fit<sup>3</sup>. In Figure 2e we report the error rates for the inferred number of  
167 clones ( $k$ ) with DPclust, pyClone (Binomial and Beta-Binomial) and sciClone. The detection of spurious extra  
168 clusters caused high uncertainty around the clone tree, with many solutions fitting the data equally well (Figure  
169 2f). We tested the effects of sequencing coverage and purity on tail detection, and found that  $\sim 100\times$  coverage

170 and high purity were required to systematically identify tails. Higher coverage is required for samples with  
171 lower purity (Extended Data Figure 1). Additional synthetic tests with complex clonal architectures confirmed  
172 the robustness of the method (Supplementary Figures 8 and 9). These analyses indicate that the previously  
173 published moderate-depth WGS studies were underpowered to detect reliable subclonal architectures, since the  
174 signal used to distinguish a tail from a subclone deteriorates with lower sequencing depth (Figure 1j). With  
175 adequate data and controlling for neutral tails, we found the correct number of clones in the large majority of  
176 tests. Not considering neutral tails led to a systematic pattern of errors that, in the worst cases, could lead to a  
177 four-fold overestimation of the number of clones.

178  
179 Not accounting for neutral tails also significantly impacts multi-region sequencing, as we discuss in the  
180 Supplementary Note. We found that multi-region bulk sequencing is affected by confounders that originate from  
181 the spatial effects of tumor growth and spatial sampling bias. In multi-sample analyses (Supplementary Note)  
182 we characterized a confounder termed the “hitchhikers mirage” (Extended Data Figure 2) caused by parts of  
183 neutral tails that spread in space, and that current methods mistake for selected subclones (Supplementary  
184 Figure 10). We also characterized two additional confounders due to the presence of locally sampled ancestors  
185 (Extended Data Figure 3) and admixing of multiple lineages (Extended Data Figure 4). These spatial  
186 confounders affect virtually all tumors (Supplementary Figures 11-13). Therefore, the joint use of MOBSTER  
187 and other heuristics is necessary to interpret subclonal deconvolution results from multi-region samples  
188 (Extended Data Figure 5, Supplementary Figure 14).

## 190 Analysis of genomic data from human samples

191  
192 We applied MOBSTER to high coverage (>100x) WGS data available in the public domain (Supplementary  
193 Note). We first re-analyzed the breast cancer sample PD1420a sequenced at ~188x from Nik-Zainal *et al.*<sup>3</sup>.  
194 Compared to the original analysis, which found 3 subclones, MOBSTER fits two subclones ( $k = 3$ ) and places  
195 a neutral tail for the lowest frequency cluster (Figure 3a). sciClone analysis of read counts for non-tail mutations  
196 confirmed  $k = 3$  Binomial clusters (2 selected subclones). Both linear and branching phylogenies could be fit to  
197 the output, with the branching tree matching the original analysis<sup>3</sup>. The cluster that MOBSTER fits to a tail  
198 appears in multiple positions of the tumor tree in the original paper after phasing<sup>3</sup>. This is consistent with our  
199 analysis, as the tail is polyphyletic, and hence composed of a mixture of descendants of the different clones. We  
200 measured the evolutionary parameters of this tumor from the fits, finding concordant estimates with our  
201 previous work<sup>16</sup>. Mutation rate was  $\mu = 3.5 * 10^{-7}$  mutations per base per tumor doubling, subclones emerged  
202 at  $t = 5.5$  (smaller subclone) and  $t = 10.4$  (larger subclone) doublings, and had selective coefficients of  
203  $s = 0.3$  and  $s = 0.66$  respectively.

204  
205 We reanalyzed the acute myeloid leukemia (AML) sample sequenced at 320x WGS by Griffith *et al.*<sup>20</sup>.  
206 MOBSTER identifies  $k = 3$  clusters (2 subclones) and a neutral tail (Figure 3b). The two subclones were also  
207 detected by Griffith *et al.*<sup>20</sup>, and were confirmed running sciClone after MOBSTER. However, MOBSTER  
208 simplified the clonal architecture by removing one spurious low-frequency “subclone”. This observation likely  
209 improves the interpretation of these data, possibly explaining why the tail was the only cluster without a clear  
210 subclonal driver mutation. Measured mutation rate was  $\mu = 9.9 * 10^{-10}$  per base per tumor doubling, subclones  
211 emerged at  $t = 22$  and  $t = 27$ , and selection coefficients were  $s = 1.3$  and  $s = 3$ , respectively.

212  
213 We also generated new multi-region WGS data (median 100x) from spatially separated regions of two primary  
214 colorectal cancers previously analyzed at lower depth in Cross *et al.*<sup>21</sup>. In tumor Set06 we analyzed high-  
215 confidence single nucleotide variants (SNVs) in diploid segments consistent across samples, and ran a  
216 comparative analysis with and without MOBSTER (Supplementary Note). The analysis with MOBSTER did  
217 not find evidence of positive subclonal selection (Figure 3c, Supplementary Figure 15), corroborated by the lack  
218 of subclonal drivers and truncal *APC*, *KRAS*, *SMAD3* and *TP53* mutations, as originally reported<sup>21</sup>. The analysis  
219 without MOBSTER would have depicted a complex subclonal structure, with several Binomial clusters  
220 consistent with multiple clone trees (Supplementary Figure 16). The analysis of Set06 gave similar results  
221 (Figure 3d, Supplementary Figure 17). Consistent with Cross *et al.*<sup>21</sup>, the clone tree depicted a tumor with only  
222 truncal driver events in *APC*, *KRAS*, *PIK3CA*, *ARID1A* and *TCF7L2*, and neutral subclonal dynamics. Again, a  
223 standard analysis would have identified a complex clonal architecture with multiple subclones (Supplementary  
224 Figure 18). Mutation rates were  $\mu = 5.6 * 10^{-7}$  for Set07, and  $\mu = 4.3 * 10^{-7}$  for Set06. Notably, orthogonal  
225 dN/dS analysis that uses the ratio of non-synonymous to synonymous mutations to detect selection<sup>22,23</sup>,  
226 confirmed the lack of evidence for positive selection at the subclonal level in those tumors (Figure 3e,  
227 Supplementary Note).

229 We also applied MOBSTER to  $n = 3$  non-small cell lung cancer samples sequenced at high depth (Figure 3f).  
230 These three tumors were those with the highest coverage and purity amongst a recently published cohort<sup>24</sup> (see  
231 also low-purity cases in Supplementary Figure 19).  
232

## 233 Neutral evolution in 2,566 whole-genomes from PCAWG

234  
235 We reanalyzed with MOBSTER one of the largest available cohorts of cancer WGS data to date, collated by the  
236 Pan-Cancer Analysis of Whole Genomes (PCAWG) international consortium and recently published in a series  
237 of studies<sup>25</sup>, including the evolutionary history of more than 2,600 cancers<sup>26</sup>. The median depth of coverage in  
238 this dataset was 45x, with median purity of 65%. According to our power analysis, data at this resolution are not  
239 suitable for reliable subclonal reconstruction (Figure 1j, 1k and Extended Data Figure 1). Figure 4a shows a  
240 PCAWG case where a standard analysis called a selected subclone. The coverage was 55x and purity 66%, with  
241 a VAF distribution similar to the down-sampled synthetic neutral cases shown in Figure 1j. With these data,  
242 MOBSTER (Figure 4b, more cases in Supplementary Figure 20) cannot fit a neutral tail in the low-frequency  
243 portion of the VAF spectrum, and instead fits a subclone (Beta component). The ground-truth is not known, but  
244 given the resolution of the data we cannot exclude the likelihood that subclonal mutations in this sample are the  
245 result of a degenerate neutral tail (see Figure 1j,k). In cases where coverage and purity were higher, MOBSTER  
246 did identify neutral tails and resolved the remaining clonal structure (Figure 4c). As expected, standard  
247 approaches would have identified spurious clusters (Figure 4d), thus compromising the whole subclonal  
248 reconstruction.  
249

250 We found widespread presence of neutral evolutionary patterns in PCAWG data using MOBSTER. We analyzed  
251 the VAF spectrum of 2,566 cancers (Supplementary Note). Theoretical population genetics predicts that, given  
252 enough power in the data, we should always expect to find a neutral tail, with or without selected subclones  
253 (Figure 2a). However, we consistently found neutral tails only in samples with higher coverage and purity  
254 (Figure 4e, red=cases with neutral tail, blue=cases without detectable tail), suggesting lack of power for  
255 subclonal inference in the majority of cases (Supplementary Figure 21).  
256

257 To further validate the presence of neutral tail mutations in this cohort, we focused on  $n = 902$  near-diploid  
258 cancers with  $>30x$  depth,  $>65%$  purity and where a tail was detected. From these cases we identified somatic  
259 mutations mapping to putative cancer driver genes<sup>25,26</sup> in neutral tails versus non-tail and performed dN/dS  
260 analysis<sup>22</sup> (Figure 4f). This orthogonal measurement confirmed that mutations in tails were likely neutral  
261 ( $dN/dS \sim 1$ ), aside from the caveats of interpreting dN/dS values in growing tumours<sup>27</sup>, whereas non-tail  
262 mutations indicated selection ( $dN/dS > 1$ ).  
263

264 We then focused on  $n = 298$  diploid cases that were found to have at least 10% of the total mutation burden in  
265 the tail, indicating sufficient power to detect the clonal architecture with confidence. We measured the  
266 proportion of tumors with a selected subclone, defined by 2 or more Binomial clusters detected from non-tail  
267 mutations. We found evidence of ongoing subclonal selection only in  $n = 9$  (3% of total, Supplementary Figure  
268 22). In the remaining  $n = 289$  cases, neutral evolutionary dynamics at the subclonal level were the adequate  
269 description of the data (Figure 4g). Lowering the threshold for proportion of tail mutations did not change the  
270 results (5% tail = 2.7% non-neutral cases; 2% tail = 3.7% non-neutral cases).  
271

272 Our analysis suggests that for the majority of PCAWG cases, the data resolution was too low to conduct robust  
273 subclonal reconstruction. Moreover, neutral tails were detectable in higher coverage and purity samples,  
274 indicating that neutral dynamics are often an adequate description of the observed subclonal heterogeneity.  
275 Standard analyses of these data therefore risk systematically mistaking neutral tails for subclonal clusters, thus  
276 inflating the complexity of the inferred subclonal architectures and producing incorrect phylogenetic trees. Our  
277 analysis using MOBSTER hence demonstrates that neutral evolutionary patterns are prevalent in PCAWG data.  
278

## 279 Analysis of longitudinal whole-genome datasets

280  
281 We analyzed a cohort of  $n = 35$  matched primary-relapse glioblastoma samples from 16 patients profiled using  
282  $\sim 100x$  WGS in a recent study by Körber et al. 2019<sup>28</sup>. Our analysis identified 9 cases characterized only by  
283 neutral evolutionary dynamics at the subclonal level in both primary and relapse, while 7 patients had a  
284 detectable ongoing subclonal expansion (Supplementary Figure 23). We found cases where positively selected  
285 subclones were unique to the primary or the relapse (Figure 5a,b), but also cases where pre-existing subclones in  
286 the primary swept through the population in the relapse, likely due to positive selection from treatment (Figure  
287 5c,d). In some cases, we found evidence of novel subclones at relapse (Figure 5e,f). MOBSTER also identified

288 clusters of mutations that were due to whole-genome duplications, as in the case of a diploid primary tumor that  
289 became tetraploid at relapse (Figure 5g,h). We note that some of the confounding effects of neutral tails in  
290 multivariate analyses (Supplementary Note) were ubiquitous in these data and would have negatively impacted  
291 standard subclonal reconstruction (Supplementary Figure 23). Orthogonal analysis with dN/dS<sup>22,23</sup> methods  
292 suggested neutral values for tail mutations (dN/dS ~1) and positive selection for others (dN/dS >1) using a panel  
293 of glioma driver genes (Figure 5h). We note that the presence of subclones under positive selection in these data  
294 was also reported in the original study<sup>28</sup>. However, using MOBSTER we obtained simplified clonal  
295 architectures, pruning some of the clusters that were due to neutral tails. Indeed, a mixture of subclonal selection  
296 and neutral evolutionary dynamics through therapy has been recently reported in a large glioblastoma study<sup>29</sup>.  
297

## 298 Discussion

299  
300 Subclonal reconstruction from cancer bulk sequencing data has paved the way to the study of cancer  
301 evolution<sup>3,30</sup>. Measurement of subclonal architectures have also clinical relevance: subclone multiplicity and  
302 other measures of intra-tumor heterogeneity have been reported as prognostic biomarkers<sup>31-34</sup>. Naturally  
303 therefore, there is the need to ensure that subclonal reconstruction is accurate.

304  
305 Here we have presented a subclonal reconstruction method that combines data-driven machine learning with  
306 theoretical population genetics. This is in contrast to purely data-driven approaches that lack an underlying  
307 evolutionary model. Recently proposed standards for subclonal reconstruction<sup>35</sup> do not account for evolutionary  
308 dynamics, and hence this recommended best practice analysis is inherently flawed.

309  
310 Moreover, we suggest that only high depth sequencing data of >90/100x is appropriate to infer subclonal  
311 architectures, and even higher depth is required for purity <75%. Subclonal reconstruction from lower depth  
312 data and lack of consideration for neutral tails risks a systematic over-calling of spurious subclones (Figure  
313 1j,k), leading to incorrect inference of the life history of tumors. These problems affects multiple previously  
314 published studies (for example refs<sup>3,34,36</sup>) and prohibit the inference of subclonal structures in the large majority  
315 of PCAWG cases. Various issues arise also in multi-region sequencing data, resulting from biases that are  
316 intrinsic to spatial sampling (Supplementary Note) and thus affect several previous studies that had insufficient  
317 depth of sequencing to infer metastatic spread (for example refs<sup>37-39</sup>). These issues also lead to inflated estimates  
318 of positive subclonal selection from VAF distributions. Single-cell sequencing removes the problem of  
319 admixing of populations<sup>40</sup>, however the underlying evolutionary dynamics described by theory remain valid for  
320 the frequency of mutations amongst the  $N$  cells sequenced<sup>41</sup>.

321  
322 The major impact of MOBSTER is that it controls for neutrally evolving cancer cell subpopulations, cleaning up  
323 the signal for downstream analyses that seek to focus on “functional” intra-tumor heterogeneity. Given the wide  
324 use of clustering methods for subclonal reconstruction, MOBSTER has the potential to impact intra-tumor  
325 heterogeneity studies that use bulk sequencing, and even that analyze the distribution of clade sizes in single-  
326 cell sequencing.

327  
328 We also highlight the limitations of the definition of “clone” in cancer as a monophyletic clade with a most  
329 recent common ancestor, noting that in the clinic we are not interested in all the ancestors of a given group of  
330 cancer cells, but only in those few ancestors that drive progression, metastasis or treatment resistance.  
331 Importantly, even under this looser definition of a clone, clustering neutral tails with Binomial models is  
332 incorrect and leads to the identification of false clones, mistaking the polyphyletic branching process that gives  
333 rise to neutral tails for a monophyletic lineage.

334  
335 This study highlights that there are intrinsic limitations to the information on tumor evolution encoded in current  
336 data, foremost because of the systematic confounding factors caused by sampling complex three-dimensional  
337 tumors. We propose that our analysis represents a step towards a more refined approach to subclonal  
338 reconstruction in bulk cancer data, a necessity for genomic-aided precision medicine.  
339

## 340 Acknowledgements

341 A.S. is supported by the Wellcome Trust (202778/B/16/Z) and Cancer Research UK (A22909). T.G. is  
342 supported by the Wellcome Trust (202778/Z/16/Z) and Cancer Research UK (A19771). We acknowledge  
343 funding from the Medical Research Council (MR/P000789/1) to A.S. and from the National Institute of Health  
344 (NCI U54 CA217376) to A.S. and T.A.G. C.P.B. acknowledges funding from the Wellcome Trust  
345 (209409/Z/17/Z). L.C. acknowledges funding by Cancer Research UK (A24566) and Children with Cancer UK

346 (17-235). This work was also supported a Wellcome Trust award to the Centre for Evolution and Cancer  
347 (105104/Z/14/Z). L.Z. is supported by the European Union's Horizon 2020 research and innovation programme  
348 under the Marie Skłodowska-Curie Research Fellowship scheme (846614). We thank Nik Matthews and the  
349 Tumour Profiling Unit at the ICR for their support with Next- Generation Sequencing. We wish to thank Verena  
350 Körber and Thomas Höfer for sharing their data and for the fruitful discussion around the glioblastoma cohort.

351

## 352 Authors contribution

353

354 GC conceived, designed and implemented the method. TH and KC developed the spatial tumor growth  
355 simulations. TH and MW generated the data for synthetic tests, which were carried out and analyzed by GC,  
356 TH, MW and DN. GC, MW and LZ analyzed the data, with input and support from WC, GDC and AA. GS, CB,  
357 TAG and AS supervised method design. LC contributed to study supervision. AS and TAG conceived and  
358 supervised the study. All authors contributed to and approved the manuscript.  
359

## 360 References (Main Text)

- 361 1. Greaves, M. & Maley, C. C. Clonal evolution in cancer. *Nature* **481**, 306–313 (2012).
- 362 2. Turajlic, S., Sottoriva, A., Graham, T. & Swanton, C. Resolving genetic heterogeneity  
363 in cancer. *Nat. Rev. Genet.* **27**, 1 (2019).
- 364 3. Nik-Zainal, S. *et al.* The life history of 21 breast cancers. *Cell* **149**, 994–1007 (2012).
- 365 4. Dentro, S. C., Wedge, D. C. & Van Loo, P. Principles of Reconstructing the Subclonal  
366 Architecture of Cancers. *Cold Spring Harb Perspect Med* **7**, a026625 (2017).
- 367 5. Roth, A. *et al.* PyClone: statistical inference of clonal population structure in cancer.  
368 *Nat Meth* **11**, 396–398 (2014).
- 369 6. Deshwar, A. G. *et al.* PhyloWGS: Reconstructing subclonal composition and evolution  
370 from whole-genome sequencing of tumors. *Genome Biol.* **16**, 35 (2015).
- 371 7. Miller, C. A. *et al.* SciClone: Inferring Clonal Architecture and Tracking the Spatial  
372 and Temporal Patterns of Tumor Evolution. *PLoS Comput. Biol.* **10**, e1003665 (2014).
- 373 8. Lynch, M. *et al.* Genetic drift, selection and the evolution of the mutation rate. *Nat.*  
374 *Rev. Genet.* **17**, 704–714 (2016).
- 375 9. Williams, M. J., Werner, B., Barnes, C. P., Graham, T. A. & Sottoriva, A.  
376 Identification of neutral tumor evolution across cancer types. *Nature Genetics* **48**, 238–  
377 244 (2016).
- 378 10. Kessler, D. A. & Levine, H. Large population solution of the stochastic Luria-  
379 Delbruck evolution model. *Proc. Natl. Acad. Sci. U.S.A.* **110**, 11682–11687 (2013).
- 380 11. Kessler, D. A. & Levine, H. Scaling solution in the large population limit of the  
381 general asymmetric stochastic Luria-Delbrück evolution process. *J Stat Phys* **158**,  
382 783–805 (2015).
- 383 12. Durrett, R. Population genetics of neutral mutations in exponentially growing cancer  
384 cell populations. *The Annals of Applied Probability* **23**, 230–250 (2013).
- 385 13. Nicholson, M. D. & Antal, T. Universal Asymptotic Clone Size Distribution for  
386 General Population Growth. *Bull Math Biol* **78**, 2243–2276 (2016).
- 387 14. Griffiths, R. C. & Tavaré, S. The age of a mutation in a general coalescent.  
388 *Communications in Statistics. Part C: Stochastic Models* **14**, 273–295 (1998).
- 389 15. Sun, R. *et al.* Between-region genetic divergence reflects the mode and tempo of  
390 tumor evolution. *Nature Genetics* **49**, 1015–1024 (2017).
- 391 16. Williams, M. J. *et al.* Quantification of subclonal selection in cancer from bulk  
392 sequencing data. *Nature Genetics* **50**, 895–903 (2018).
- 393 17. Hartl, D. L. & Clark, A. G. *Principles of Population Genetics*. (Sinauer Associates,  
394 Inc., 2006).
- 395 18. Luria, S. E. & Delbrück, M. Mutations of bacteria from virus sensitivity to virus  
396 resistance. *Genetics* **28**, 491–511 (1943).

- 397 19. Graham, T. A. & Sottoriva, A. Measuring cancer evolution from the genome. *J.*  
398 *Pathol.* **241**, 183–191 (2017).
- 399 20. Griffith, M. *et al.* Optimizing Cancer Genome Sequencing and Analysis. *Cell Systems*  
400 **1**, 210–223 (2015).
- 401 21. Cross, W. *et al.* The evolutionary landscape of colorectal tumorigenesis. *Nat. ecol.*  
402 *evol.* **2**, 1661–1672 (2018).
- 403 22. Martincorena, I. *et al.* Universal Patterns of Selection in Cancer and Somatic Tissues.  
404 *Cell* **171**, 1–13 (2017).
- 405 23. Zapata, L. *et al.* Negative selection in tumor genome evolution acts on essential  
406 cellular functions and the immunopeptidome. *Genome Biol.* **19**, 924 (2018).
- 407 24. Lee, J. J.-K. *et al.* Tracing Oncogene Rearrangements in the Mutational History of  
408 Lung Adenocarcinoma. *Cell* **177**, 1842–1857.e21 (2019).
- 409 25. The ICGC/TCGA Pan-Cancer Analysis of Whole Genomes Consortium. Pan-cancer  
410 analysis of whole genomes. *Nature* **578**, 82–93 (2020).
- 411 26. Gerstung, M. *et al.* The evolutionary history of 2,658 cancers. *Nature* **578**, 122–128  
412 (2020).
- 413 27. Williams, M. J. *et al.* Measuring the distribution of fitness effects in somatic evolution  
414 by combining clonal dynamics with dN/dS ratios. *eLife Sciences* **9**, 612 (2020).
- 415 28. Körber, V. *et al.* Evolutionary Trajectories of IDHWT Glioblastomas Reveal a  
416 Common Path of Early Tumorigenesis Instigated Years ahead of Initial Diagnosis.  
417 *Cancer Cell* **35**, 692–704.e12 (2019).
- 418 29. Barthel, F. P. *et al.* Longitudinal molecular trajectories of diffuse glioma in adults.  
419 *Nature* **135**, 1–9 (2019).
- 420 30. Shah, S. P. *et al.* The clonal and mutational evolution spectrum of primary triple-  
421 negative breast cancers. *Nature* **486**, 395–399 (2012).
- 422 31. Andor, N. *et al.* Pan-cancer analysis of the extent and consequences of intratumor  
423 heterogeneity. *Nat. Med.* **22**, 105–113 (2016).
- 424 32. Morris, L. G. T. *et al.* Pan-cancer analysis of intratumor heterogeneity as a prognostic  
425 determinant of survival. *Oncotarget* **7**, 10051–10063 (2016).
- 426 33. Jamal-Hanjani, M. *et al.* Tracking the Evolution of Non-Small-Cell Lung Cancer. *New*  
427 *England Journal of Medicine* **376**, 2109–2121 (2017).
- 428 34. Espiritu, S. M. G. *et al.* The Evolutionary Landscape of Localized Prostate Cancers  
429 Drives Clinical Aggression. *Cell* **173**, 1003–1013.e15 (2018).
- 430 35. Salcedo, A. *et al.* A community effort to create standards for evaluating tumor  
431 subclonal reconstruction. *Nature Biotechnology* **38**, 97–107 (2020).
- 432 36. Yang, L. *et al.* An enhanced genetic model of colorectal cancer progression history.  
433 *Genome Biol.* **20**, 1–17 (2019).
- 434 37. Yates, L. R. *et al.* Genomic Evolution of Breast Cancer Metastasis and Relapse.  
435 *Cancer Cell* **32**, 169–184.e7 (2017).
- 436 38. Gundem, G. *et al.* The evolutionary history of lethal metastatic prostate cancer. *Nature*  
437 **520**, 353–357 (2015).
- 438 39. Noorani, A. *et al.* Genomic evidence supports a clonal diaspora model for metastases  
439 of esophageal adenocarcinoma. *Nature Genetics* **347**, 1–10 (2020).
- 440 40. Navin, N. E. The first five years of single-cell cancer genomics and beyond. *Genome*  
441 *Res.* **25**, 1499–1507 (2015).
- 442 41. Chkhaidze, K. *et al.* Spatially constrained tumour growth affects the patterns of clonal  
443 selection and neutral drift in cancer genomic data. *PLoS Comput. Biol.* **15**, e1007243  
444 (2019).



445

446

447

## Figure Legends

448

449

450

451

452

453

454

455

456

457

458

459

460

461

462

463

464

465

466

467

468

469

470

471

472

473

474

475

476

477

478

479

480

481

482

483

484

485

486

487

488

489

490

491

492

493

494

495

496

497

498

499

500

501

502

503

504

505

506

507

508

509

510

511

512

513

514

515

**Figure 1. Theoretical predictions of cancer genomic data under different evolutionary dynamics.** (a) A tumor formed by a single “functionally monoclonal” expansion follows neutral evolutionary dynamics driven only by mutation and drift. (b) The clone tree can be represented as a single “truncal” clone. (c) In diploid regions, the Variant Allele Frequency (VAF) distribution is characterized by one clonal cluster and a neutral  $1/f^2$  tail of subclonal mutations. (d) In a tumor with one subclone under positive selection (functionally polyclonal) the evolutionary forces of mutation and drift are still at play within each clone. (e) The clone tree is represented as a truncal node giving rise to a selected subclone within it. (f) The VAF shows one extra cluster due to subclonal mutations in the subclone that have risen in frequency due to selection. (g,h) Standard subclonal deconvolution identifies clusters of neutral tail mutations that are not subclones, as they represent admixed polyphyletic lineages. (i) This causes inflated estimates of the number of clones that propagate errors and uncertainty downstream, with several incorrect phylogenetic trees fitting the data. (j) In these synthetic examples, the VAF distribution of a tumor with and without subclonal selection changes for different values of coverage and purity, affecting the ability to observe neutral tails. A neutral tail (grey) becomes difficult to detect at 40x depth. (k) The “degenerated tail” at 40x can be statistically indistinguishable from a positively selected subclonal cluster. Data at such resolution are not powered to distinguish true positive subclonal selection from neutral tail mutations.

**Figure 2. Model-based tumor subclonal reconstruction.** (a) MOBSTER combines a Pareto Type-I distribution with  $k$  Beta random variables into a univariate finite mixture with  $k + 1$  components. The Pareto captures the frequency spectrum of neutral mutations predicted by theory (Landau distribution decaying as  $1/f^2$ ), whereas Beta components detect alleles under positive selection. The histogram shows clustering assignments for a tumor with one selected subclone ( $k = 2$ ). (b) MOBSTER filters out neutral tail mutations, and one can cluster the rest with any tool for subclonal reconstruction using read counts. CCF, cancer cell fraction. (c, d) MOBSTER applied to the examples in Figure 1a,b detects the clusters corresponding to the true selected clones, hence recovering the correct clonal architecture. WGS, whole genome sequencing (e,f) We used synthetic 120x WGS data from  $n=150$  simulated tumors to compare current methods with MOBSTER (plots show mean and inter quartile range IQR, upper whisker is 3rd quartile  $+1.5*IQR$  and lower whisker is 1st quartile  $-1.5*IQR$ ). We measured how many clusters (e) and clone trees we identify (f). Tests compare Binomial mixtures from DPclust, pyClone and sciClone, and Beta-Binomial mixtures from pyClone, parameterized by concentration  $\alpha > 0$ . DPclust and pyClone learn  $\alpha$  from the data assuming a Gamma prior. sciClone is a variational method with hardcoded  $\alpha$ . In (e) we report the logarithm of the ratio between the number of subclones found by MOBSTER ( $k_{fit}$ ) and the true number of clones ( $k_{true}$ ). Red dashed line represents  $k_{fit} = k_{true}$ . In (f) we plot the number of trees that can be fit by pigeonhole principle using the output of each tool.

**Figure 3. Analysis of single sample and multi-region whole-genome data.** (a) Breast carcinoma  $\sim 180x$  WGS sample from ref<sup>3</sup>. MOBSTER identified a neutral tail plus  $k = 3$  Beta clusters (2 subclones, consistent with two clone trees). Analysis of non-tail mutations with sciClone confirmed 2 subclones. sciClone without MOBSTER would have fit one extra clone to the tail. Non-parametric bootstrap is used to estimate the 95% bootstrap confidence intervals for the parameters. (b) Leukemia  $\sim 320x$  WGS sample from ref<sup>20</sup>. MOBSTER found two subclones ( $k = 3$ ), confirmed with sciClone, and 2 clone trees. (c) WGS data at 100x from 4 biopsies of colorectal cancer Set07. From VAF of diploid mutations we identified neutral tails and no subclonal selection; from non-tail mutations we found 5 clusters (multivariate clustering with  $\alpha = 10^{-6}$ , Supplementary Note). C1 is the truncal cluster; all other clusters are enriched mutations private to a biopsy, indicating ancestor effect (Supplementary Note). The clone tree depicts a neutrally expanding tumor with all drivers in the trunk. Analysis without MOBSTER would have inflated the number of subclones (right panel; Supplementary Figures 20-23). (d) WGS data at 100x from 6 biopsies of cancer Set06 also showed neutral subclonal dynamics. Without MOBSTER we would have inflated the number of selected subclones (right panel; Supplementary Figures 24-27). (e) dN/dS analysis for Set06 and Set07 comparing truncal vs subclonal mutations confirmed lack of evidence for positive selection at the subclonal level, corroborating our conclusions. (f) Three lung cancer cases from ref<sup>24</sup> sequenced at 100x WGS were consistent with neutral subclonal dynamics.

**Figure 4. Analysis of 2,566 whole-genomes from PCAWG with MOBSTER.** (a) Fit of a PCAWG<sup>25</sup> tumor with 55x coverage and 66% purity using standard methods. (b) At this data resolution, neutral tails are under-sampled (Figure 1j,k) and cannot be distinguished from selected subclones. (c) In PCAWG cases with higher coverage (67x) and purity (74%), neutral tails can be clearly detected using MOBSTER. (d) Analysis of the same tumor with standard methods would have identified multiple subclonal clusters, including a cluster of neutral tail mutations. (e) We analyzed  $n=2,566$  PCAWG samples, plotted here for purity vs coverage. Blue dots are tumors where MOBSTER cannot fit a tail. Red cases have a neutral tail. Percentage of tail mutations determines dot size. The marginal histograms report the normalized number of cases with tail. (f) We focused on the 902 diploid cases with coverage  $>30x$  and purity  $>65\%$  (median of the cohort) where we could fit a tail. Using a panel of 191 pan-cancer driver genes, we show that tail mutations have  $dN/dS \sim 1$ , providing no evidence of positive selection (point estimate and Confidence Intervals from `dndscv`). Clonal and subclonal non-tail mutations show  $dN/dS > 1$ , consistent with positive selection. (g) If we take the 298 diploid cases with a tail containing at least 10% of the total mutational burden, we find evidence of a selected subclone only in 9 cases (3% of tumors). Similar proportions are obtained if we impose a 5% or 2% cutoff on the size of the tail. See Supplementary Figures 29-31.

**Figure 5. Analysis of longitudinal glioblastoma samples with MOBSTER.** (a). Patient H043-BU96 is one of  $n = 16$  IDH-wildtype glioblastomas for which we analyzed WGS data ( $\sim 100x$ ) from pre-treatment and post-treatment longitudinal samples previously generated<sup>28</sup>. (b) Analysis following MOBSTER identified subclones private to the primary (yellow) and relapse (green) tumor respectively, the latter containing a putative driver mutation in LINC00689. (c) Patient H043-KZWs MOBSTER fits. (d) Here a subclone detected in the primary went on to sweep through the relapse, which was hypermutant after temozolomide treatment (zoom-in logscale panel). (e) Patient H043-PWC258 MOBSTER fits. (f) Here the primary sample showed neutral evolutionary dynamics, whereas the relapse contained detectable subclones possibly mixing with the neutral tail. An additional high-frequency subclone was detected from a downstream analysis using Binomial clustering of read counts (purple cluster, split into 2 Binomial components). (g) MOBSTER can also be used to identify and assign clusters that are produced by whole-genome duplications, or more general aneuploid states. In such contexts, we expect to see peaks in the VAF distribution that distinguish mutations that happened before and after genome doubling. In the case of patient H043-6F91, a diploid primary tumor (neutral) became whole-genome duplicated at relapse. (h) Orthogonal dN/dS analysis (point estimate and Confidence Intervals from `dndscv`) of mutations in 74 putative GBM driver genes assigned to neutral tails versus non-tail provided evidence of selection only in non-tail mutations. The full list of analyzed cases is available in Supplementary Figure 32.

517 **Online Methods**

518

519 **Model-based clustering of cancer subclonal populations with MOBSTER**

520

521 The subclonal deconvolution problem is popular in the cancer literature<sup>35</sup>. Given read counts for a list of  
 522 mutations detected from bulk sequencing of multiple tumor samples, we want to detect clusters of mutations  
 523 that represent cancer subpopulations admixed in our samples. The problem can be framed to include any type of  
 524 somatic mutation for which we can estimate the frequency, in the data, of the somatic (i.e., alternative) allele.  
 525 Usually, the mutations that are easier to call are Single Nucleotide Variants (SNVs); more complex structural  
 526 variations or insertion-deletions are more challenging to determine accurate allelic frequencies. Regardless  
 527 mutation types, our aim is to use determine mutations clusters that suggest cancer subpopulations (i.e., clones)  
 528 under positive selection.

529

530 MOBSTER is a mixed method that combines two types of random variables to approach this problem.

531

532 **The frequency spectrum and the observational process.** Kessler and Levin<sup>10</sup> have shown that, in the large  
 533 population solution of the stochastic Luria-Delbrück model, the probability of having  $m$  mutants follows a fat-  
 534 tail Landau distribution

535

$$p(m) = \frac{1}{\mu N} f_{\text{Landau}} \left( \frac{m}{\mu N} - \log \mu N + \gamma - 1 \right).$$

536

537 Here  $N$  is population size,  $\mu$  the average fraction of birth events and  $\gamma$  the Euler constant. The asymptotic  
 538 behavior of  $f_{\text{Landau}}$  can be approximated as  $f_{\text{Landau}}(x) = 1/x^2$ , which leads to the power-law approximation that  
 539 has also been derived by others<sup>12-14</sup> as  $p(m) \approx 1/m^2$ .

540

541 A generative model for this power law can be constructed with a standard Markovian stochastic birth-death  
 542 process of cell division – sometimes called *branching process*<sup>16</sup>. The existence of patterns of neutral evolution is  
 543 thus a consolidated result from Population Genetics arguments that describe the spread of alleles in growing  
 544 populations without recombination, such as cancer<sup>17</sup>. In other words, the *progeny of each clone* accumulates  
 545 neutral passenger mutations until any of their daughter cells acquires a new mutation that undergoes selection  
 546 because it triggers a new clonal expansion with increased fitness: the power-law spectrum emerges therefore by  
 547 the frequencies of passengers. When a daughter cell enjoys a clonal expansion, however, the frequency of the  
 548 variant alleles that accrued from the ancestor cell to the actual cell that acquired the driver, will grow.  
 549 Eventually, this new subclonal expansion will become detectable if selection forces are strong compared to  
 550 background (which is the clone within this cell was born). In a recursive fashion, the progeny of this new cell/  
 551 subclone will start dividing, giving rise to another power-law distributed tail of within-clone neutral dynamics.  
 552 Example subclonal evolutionary dynamics are shown in the vignette “1. Example subclonal dynamics”  
 553 (Supplementary Data), where we animate a subclonal expansion which shows how subclones emerge from low  
 554 frequency up until they sweep, and how the allele frequency distribution changes over time.

555

556 Importantly, we want to make it clear that the power-law part of the spectrum – i.e., the *tail* – results from the  
 557 accumulation of passenger mutations in the progeny of each clone. We note that this result – in particular the  
 558 exponent 2 (shape) – refers to the total population structure of the tumor, which is accessible only in the  
 559 theoretical scenario in which we can sequence all the cancer cells. Therefore, any specific finite sample that we  
 560 collect and sequence, which is also contaminated by normal cells, might exhibit deviations from this theoretical  
 561 distribution<sup>16</sup>. Deviations from strict exponential growth – e.g., due to spatial constrains – can also cause  
 562 theoretical deviations from the exponent two<sup>13,42</sup>. However, we use this result to create a parametric model-  
 563 based approach to analyze cancer data (i.e., we fix the type of distribution, but not its parameters).

564

565 **Input data and conceptualization.** We work with sequencing data for the variant alleles of  $n$  somatic  
 566 mutations, which we can pre-process in different ways. One option is to adjust Variant Allele Frequency (VAF)  
 567 values for copy number and purity, retrieving the so-called Cancer Cell Fractions (CCF) and re-scaling them  
 568 into  $[0, 1]$  by halving the CCF. With these adjusted VAF values we expect a clonal peak at roughly 50% VAF,  
 569 with outliers spreading around 0.5 but well below 1; compared to CCF, these values avoid the truncation of  
 570 values above 1<sup>3</sup>. Another similar option is to adjust VAF values only by copy number, obtaining the so-called  
 571 Cellular Prevalence (CPs). A third option is using directly the raw VAF data; in this last scenario we can further  
 572 split mutations by karyotype – i.e., the absolute copy number segments where they map to – and account for the

573 fact that different aneuploidy states have different expected distributions (e.g., a triploid tumor is expected to  
574 have two peaks of mutations, plus a tail and possibly subclonal clusters).  
575

576 On real data, we suggest to use mutations that map to copy number segments with common karyotypes (i.e.,  
577 copy states), such as diploid regions (with or without loss of heterozygosity), and triploid and tetraploid  
578 segments. Mutations mapping to more complex karyotypes (e.g., highly amplified oncogenes) can always be  
579 mapped post hoc, after clustering, and should account for a small subset of the tumor’s mutational burden. We  
580 stress to use mutations in high-confident copy-number regions to carry out subclonal deconvolution; miscalled  
581 copy number states confound the inference creating artifact clusters of mutations. As a best practice, we usually  
582 attempt a first fit using diploid genomes without losses of heterozygosity (i.e., regions with one copy of the  
583 major and minor alleles), where we can identify high-confidence diploid SNVs.  
584

585 Regardless the representations, a model for the *frequency spectrum*  $\rho$  of the observed mutations with  $k \geq 1$   
586 detectable clones is a random variable that follows  
587

$$\rho \sim \sum_{i=1}^k (Y_i + B_i),$$

588  
589 where

- 590 •  $Y_i \propto x^{-\alpha}$  is a power-law random variable for frequencies of neutral mutations in the progeny of clone  
591  $i$ . The generic exponent  $\alpha > 0$  gives flexibility to accommodate all the confounders described above;
- 592 •  $B_i \in [0,1]$  is a Beta random variable modelling the signal of clone  $i$ . In layman terms,  $B_i$  models the  
593 “peak” in the VAF distribution due to the hitchhikers of the clone. These distributions range in  $[0,1]$ ,  
594 rendering them suitable to describe allelic frequencies (and also motivating why we scale CCF values  
595 to fit this range). For the sake of simplification, we assume here to work with adjusted VAF values, so  
596 that aneuploidy states (amplified, unamplified) are adjusted to form a single peak in the distribution  
597 (i.e., exactly as with CCF).  
598

599 This model looks simple, and further observations are required to turn it into a mixture of standard random  
600 variables. In this formulation, the random variables for the tail and the bump of a clone are coupled to capture a  
601 joint signal. While the overall mixing proportions can be assumed to be independent, this compound random  
602 variable requires an extra level of mixing within each clone – i.e., another mixing weight to properly capture the  
603 proportions of the clone tail, and bump. We can however simplify this model accepting to track at finer detail  
604 only the clusters of each clone, which we use to identify subpopulations in the frequency spectrum (i.e., we use  
605 the clone’s peak, obtained from the cluster’s mean, to assess the phylogenetic history of the tumor).  
606

607 We therefore simplify the model by noting that all tails have the same exponent  $\alpha > 0$ , which holds if all clones  
608 have the same mutation rate. If the mutation rate does not change among subclones – i.e., when there are no  
609 hypermutant subclones – all tails are described by the same theoretical distribution, and can be represented as  
610 multiple instances of the same random variable. Thus, we group them together in a single power-law tail  
611

$$\rho \sim \left( Y + \sum_{i=1}^k B_i \right).$$

612  
613 Here the random variables have the same meaning as above, but the clone is no longer indexed by  $i$ . This model  
614 has a key advantage over the one where each clone “emits” its own tail: the random variables are decoupled and  
615 allow a simple mixture-model formulation which we will present below.  
616

617 Before concluding, we observe that given  $\rho$ , the *observational model* for read counts collected from NGS  
618 sequencing, is a standard binomial process  $n|\rho, m \sim \text{Bin}(n|m, \rho)$ , where  $m$  is the coverage (total number of  
619 reads), and  $w$  the number of reads harboring the variant allele;  $\rho$  is then the success probability for  $m$  iid  
620 Bernoulli trials. It is important to observe that the frequency spectrum and the observational process look at the  
621 data from different perspectives: the former is a distribution on allelic frequencies, while the latter on read  
622 counts. In this observational model we can in principle use Beta-Binomial distributions to account for coverage  
623 overdispersion.  
624

625 **Relation to other models in the literature.** The literature is rich with models that describe the above  
626 observational process and variation thereof, either with Binomial or Beta-Binomial distributions. We briefly  
627 discuss those that are more related to our framework.

628  
629  
630  
631  
632  
633  
634  
635  
636  
637  
638  
639  
640  
641  
642  
643  
644  
645  
646  
647  
648  
649  
650  
651  
652  
653  
654  
655  
656  
657  
658  
659  
660  
661  
662  
663  
664  
665  
666

Bayesian methods that employ Dirichlet Processes for infinite Binomial mixture models are a popular generalization of the observational process. These non-parametric methods can fit an unspecified number of clusters  $k$  to data, simplifying model selection procedures. pyClone<sup>5</sup>, DPclust<sup>3</sup> and PhyloWGS<sup>6</sup> are three popular tools for clonal deconvolution that in different ways use this framework. pyClone and DPclust implement Binomial mixtures, with the former also supporting Beta-Binomial distributions; in both cases a stick-breaking construction for Dirichlet Process priors is adopted<sup>43</sup>. PhyloWGS, instead, combines Binomial distributions with a tree stick-breaking construction for the Dirichlet Process priors<sup>44</sup>, which allows PhyloWGS to cluster jointly the input SNVs, and construct a phylogenetic tree for the detected clones.

An alternative popular approach based on finite mixture models is SciClone<sup>7</sup>, which supports Binomial, Beta and Gaussian mixtures. SciClone fits the models to data via Variational Inference, an information-theoretic approach to approximate the posterior distribution over the model's parameters. SciClone is a hybrid tool, as it can cluster allelic frequencies via Beta/ Gaussian mixtures, and read counts via Binomial mixtures. We want to note that, with Beta distributions, canonical Bayesian modeling leads to intractable priors, even if the conjugate prior distribution of the Beta distribution can be found by following the principles of conjugate priors for the exponential family. For this reason, Variational Inference of Beta mixtures exploits a Gamma approximation to the prior and posterior distributions, originally derived by Mao and Li<sup>45</sup>. In this approximation we cannot derive the so-called evidence lower bound, a standard measure to monitor convergence of a variational fitting algorithm.

These models are related to MOBSTER's framework: they assume that  $\rho$  can be approximated by a point-process (e.g. a Dirac distribution) centered at the Beta means. The potential pitfall is clear: by applying the observational process to neutral mutations, the number of clones is overestimated. Clusters will be called from tail mutations (polyphyletic lineages), which is wrong when we look for clones under selection. We note that SciClone with Beta distributions models the allele frequency spectrum as well, however, they do not account for power-law tails of neutrally-evolving mutations.

**Distributions and likelihood.** MOBSTER implements a statistical model to fit  $n$  VAF values to  $Y$ , the tail, and to any one of the  $B_i$  Betas, the clones (predefined in number). From a fit, tail mutations can be removed inspecting clustering assignments, and other methods can be used to fit the observational process on the read counts of the remaining data. For this reason, MOBSTER is complementary to the tools mentioned above, as it works upstream the observational process. Nonetheless, our method provides also a preliminary indication on the possible number of subclones in the tumor: with high-quality data with low dispersions, one can expect the same number of clones to be confirmed by downstream analysis of non-tail mutations.

The fit uses a pre-specified number of  $k + 1$  components, where  $Y$  is a Pareto Type-I distribution as the power-law tail. For a scale  $x_*$  and shape  $\alpha > 0$ , its density is

$$g(x | x_*, \alpha) = \alpha x_*^\alpha \frac{1}{x^{\alpha+1}}$$

667  
668  
669  
670  
671  
672

for  $x > x_*$ , and 0 otherwise. Notice that the density is 0 for values below the scale parameter, which requires a sharp cutoff on the input VAF, and that its support is  $[0, +\infty)$ . The model also uses  $k$  Beta distributions  $B_1, \dots, B_k$  to model clonal and subclonal clusters. For a shape  $a > 0$  and  $b > 0$  the density of a Beta random variable is

$$h(x|a, b) = \frac{x^{a-1}(1-x)^{b-1}}{B(a, b)}$$

673  
674  
675  
676  
677  
678  
679  
680

where  $B(a, b) = \int_0^1 x^{a-1}(1-x)^{b-1} dx$  is the beta-function. The support of this distribution is  $[0, 1]$ , the full frequency spectrum.

The overall model uses a Dirichlet prior on the abundance of each clone; thus MOBSTER is a Finite Dirichlet Mixture Model with both Beta and Pareto distributions. The model likelihood for a dataset  $X = \{x_i | i = 1, \dots, n\}$  where we assume each  $x_i$  to be iid, is a combination of two types of densities

$$p(D|\theta, \pi) = \prod_{i=1}^n \left[ \pi_1 g(x_i | x_*, \alpha) + \sum_{w=2}^k \pi_w h(x_i | a_{w-1}, b_{w-1}) \right].$$

681

682

We use  $\theta$  as a shorthand to the model parameters, and  $\pi = [\pi_1 \dots \pi_{k+1}]$  for the mixing proportions – a standard Dirichlet variable on the  $(k + 1)$ -dimensional probability simplex. Notice that, just for notational convenience, we are assuming that the first model component is the Pareto random variable (the tail); we hold this setup fixed even if the model does not fit a tail (in that case we force  $\pi_1 = 0$ ). Because of this, we use the index  $w - 1$  for the parameters of the Beta distributions just to reflex that their index start from one.

687

688

**Fitting MOBSTER.** The formulation uses  $n \times (k + 1)$  latent variables  $\mathbf{z}$ . A variational approach to fit this mixture is theoretically possible: we could use conjugate Gamma priors for the Pareto, and we would approximate the posteriors for the Beta components as in sciClone. However, we could only approximate a criterion for convergence of the fit, as mentioned above.

689

690

691

692

693

We fit the model parameters via Maximum Likelihood Estimation (MLE) through an adaptation of a standard Expectation-Maximization approach (EM). This alternative is faster than a Bayesian Monte Carlo strategy, at the drawback of inferring a point estimate of the parameters. The lack of an explicit measure of uncertainty in the prediction (confidence) can be mitigated using the bootstrap.

694

695

696

697

698

We perform these steps to fit a MOBSTER model. In the E-step, we compute the posterior estimates of the latent variables as usual, once we account for the two different distributions involved

699

700

$$z_{w,1} | \theta \propto \pi_1 g(x_i | x_*, \alpha) \quad z_{w,i} | \theta \propto \pi_i h(x_w | a_i, b_i)$$

701

In both cases the normalisation constant  $C_w$  is the overall density mass for point  $x_w$

702

$$C_w = \pi_1 g(x_w | x_*, \alpha) + \sum_{i=2}^k \pi_i h(x_w | a_i, b_i).$$

703

In the M-step, for the Pareto tail, we begin by noting that the scale  $x_*$  of the distribution can be set to its MLE<sup>46</sup>, which is known to be the smallest observed frequency  $x_* = \min X$ . This is a constant of the data, so we have one less parameter to fit. We fit the Pareto shape  $\alpha$ , given  $x_*$ ; switching to the log-likelihood and including latent variables its MLE estimator is

704

705

706

707

$$\alpha_{\text{MLE}} = - \frac{\sum_{i=1}^n z_{i,1}}{\sum_{i=1}^n z_{i,1} \log(x_*/x_i)}$$

708

For the Beta clones, in the M-step, the MLE estimator for the distributions has no closed form; we can resort to approximate it numerically, increasing the computational burden. We can also rely on a recent analytical result on the Moment-Matching (MM) estimator of mixtures of Betas by Schröder and Rahmann<sup>47</sup>. MM consists in matching  $t$  empirical moments of the data  $X$  to the theoretical moments of the distribution, and solving for them. Here  $t = 2$  (mean and variance); a Beta distribution has mean  $\mu$  and variance  $\sigma$  given by

709

710

711

712

713

714

$$\mu = \frac{a}{a+b} \quad \sigma = \frac{ab}{(a+b)^2(1+a+b)}.$$

715

For a Beta, conditioned on the latent variables, the MM estimator is

716

717

$$\mu_{i\text{MM}} = \frac{\sum_{w=1}^n z_{w,i} x_w}{n\pi_i} \quad \sigma_{i\text{MM}} = \frac{\sum_{w=1}^n z_{w,i} (x_w - \mu)^2}{n\pi_i}.$$

718

Given estimates for  $\mu_i$  and  $\sigma_i$ , we can re-parametrize the Beta as

719

720

$$a_{i\text{MM}} = \left( \frac{1 - \mu_i}{\sigma_i} - \mu_i^{-1} \right) \mu_i^2 \quad b_{i\text{MM}} = \mu_i (\mu_i^{-1} - 1).$$

721

We remark that MM is not the same as computing the MLE, which computes the zeroes of the derivative of the likelihood with respect to the parameters  $\theta$ ,  $\partial h / \partial \theta$ . Thus, the properties of standard EM do not hold when we compute updates via MM: we cannot guarantee that the likelihood increases monotonically, because we cannot employ Jensen's inequality. It is however shown<sup>47</sup> that the differences between the estimators are negligible in most cases. For the sake of precision, Schröder and Rahmann propose to call a fit through the MM for Beta distributions the “iterative method of moments”, rather than EM.

722

723

724

725

726

727

728  
729  
730  
731  
732  
733  
734  
735  
736  
737  
738  
739  
740  
741  
742  
743  
744  
745  
746  
747  
748  
749  
750  
751  
752  
753  
754  
755  
756  
757  
758  
759  
760  
761  
762  
763  
764  
765  
766  
767  
768  
769

In MOBSTER's implementation we provide both a standard EM fit with numerical solution for the MLE of Beta distributions, and the faster iterative method of moments. In the former case we monitor convergence of the likelihood, as standard. In the latter we use the posterior estimates of  $\boldsymbol{\pi}$  since the likelihood is not monotonically increasing. A theoretical property of this MM approach is that, in each step, before updating the component weights, the expectation of the estimated density equates the sample mean. In particular, this is true at a stationary point; a proof of this is in Lemma 1 of Schröder and Rahmann<sup>47</sup>.

**Initial conditions.** As standard in EM approaches, we compute the fit with several random initial conditions. We provide two heuristics to compute the initial condition of the fit (Supplementary Figure 1). One is based on a peak detection heuristic applied in the frequency range  $[0.1, 1]$  to VAF values binned with size 0.01. To detect  $k$  initial peaks we perform kmeans clustering of each peak's  $x$ -coordinate, and store their centres. If there are  $w < k$  peaks to cluster, we sample  $k - w$  random values in  $(0, 1)$  for the remaining peaks. We use the centers of these clusters as the mean of  $k$  Beta distributions with randomized variance sampled in  $[10^{-3}, 0.25]$ ; we do sample variance values until the corresponding Beta parameters  $a$  and  $b$  are positive. For the tail,  $\alpha$  is randomly sampled in the interval  $[0.01, 5]$ . These values provide wide ranges of different initial distributions. An alternative method to select the initial condition of the fit is totally randomized.

Experimental results show that peak detection is a more robust initialization method; the random counterpart sometimes leads to Beta distributions with mean approaching one, a region of parameter values where the likelihood becomes less stable, leading to numerical difficulties. In many cases, we test fits with both initial conditions and retain the best one.

**Clustering assignments and model selection.** We do not want the fit to be biased towards tails, as we would miss low-frequency subclones that hide in the tail. Besides, simulations suggest limits to the detectability of tails, and therefore we shall not assume tail to be always present in the data. For this reason, MOBSTER can "turn off" the Pareto component of the mixture (i.e., setting  $\pi_1 = 0$ ) and fit just  $k$  Beta. Hence, we can perform model selection for  $1 \leq k \leq K$  considering both models with and without a tail. This induces a statistical competition and allows us to select the model that best explains the data, with or without a tail.

In MOBSTER we compute the negative log-likelihood  $NLL = -\log f(X | \boldsymbol{\theta}, \boldsymbol{\pi})$  of the data, which we use to derive the usual AIC and BIC scores  $BIC = 2NLL + |\boldsymbol{\theta}| \log n$ , and  $AIC = 2NLL + 2|\boldsymbol{\theta}|$ .

These criteria favor simpler fits by penalizing a model for the number of its parameters  $|\boldsymbol{\theta}|$ . A model with  $k$  Beta distributions and one tail has  $|\boldsymbol{\theta}| = 3k + 2$  parameters ( $k + 1$  for the Dirichlet mixture  $\boldsymbol{\pi}$ ,  $2k$  for the Beta(s) and 1 for the Pareto tail). The fit without tail model has  $|\boldsymbol{\theta}| = 3k - 1$  parameters; fewer parameters reduce less the penalty, thus favoring fits without a tail.

In MOBSTER we want to drive the fit to select separate clusters, i.e., fits with few overlapping components, which we do not achieve using BIC or AIC. We achieve these separations by using instead two types of entropy terms. In one case we compute, from the latent variables, the usual entropy  $H(\mathbf{z})$

$$H(\mathbf{z}) = \sum_{i=1}^{k+1} \sum_{j=1}^n z_{i,j} \log z_{i,j}$$

770  
771  
772  
773  
774  
775  
776  
777  
778  
779  
780  
781  
782  
783

and obtain the standard Integrative Classification Likelihood (ICL)  $ICL = BIC + H(\mathbf{z})$ , approximated through the BIC<sup>48</sup>. In this paper we also introduce a heuristic variation to the ICL, which we call reICL, a reduced-entropy criterion where we use the entropy of mutations that are not assigned to a tail (Supplementary Figure 1). This is defined as  $reICL = BIC + H(\hat{\mathbf{z}})$ , where  $\hat{\mathbf{z}}$  are the latent variables for the set of mutations  $\{x | 1 \neq \operatorname{argmax} \mathbf{z}_{x,\cdot}\}$ , re-normalized. Notice that in practice  $\hat{\mathbf{z}}$  is defined from the hard clustering assignments that we use to assign mutations to clusters; cluster "1" is the label to identify tail mutations.

Entropy terms in ICL and reICL help to fit separate clusters because overlapping mixture components have higher entropy, and therefore penalty. The maximum entropy distribution is the uniform one, which is when we cannot confidently assign mutations to clusters (a point seems to be equally-well explained by multiple components). By definition, ICL will push towards fits with a clear separation among tail *and* Beta components, while reICL will only require separation of the Beta ones. This modification to the ICL seems reasonable because the Pareto tail overlaps - by definition - to all subclonal clusters, and this leads to strong entropy penalizations with

784 ICL. For this reason, ICL will be more stringent in calling tails than reICL, which drops a part of the entropy  
785 penalty restricting its computation to  $\hat{z}$ . See also Supplementary Figure 1 for a graphical explanation.

786

787 Notice that, because we are using NLL, we seek to *minimize* these scores. In the tests, we investigate different  
788 model-selection strategies, and choose as default score for model selection in MOBSTER reICL, which seems to  
789 provide a nice tradeoff. Between the ability to identify the Beta components, while retaining the tail structure.

790

## 791 Analysis of synthetic data

792

793 In the Supplementary Note and in the Supplementary Data (vignettes “Simulated single-sample data analysis”  
794 and “Simulated multi-sample data analysis”) we explain how we used branching processes to generate tumors  
795 without and with space, and present output metrics to assess precision and sensitivity of our analyses (number of  
796 clusters, confidence in the predictions, rates of false/true positives/negatives, the effect of coverage and purity  
797 and the ability to identify subclones). In the tests we used MOBSTER and other tools for subclonal  
798 deconvolution.

799

800 We found MOBSTER and the analyses built around it to be accurate, across all simulated tumors. In all cases tails  
801 improve fit quality, from a statistical point of view. This clustering problem is challenging because tails and  
802 clones overlap, confounding weak signals of subclonal selection at the low-frequency VAF. We used our  
803 performance and combinations of coverage and purity to identify minimum requirements for reliable  
804 deconvolution in non-spatial data. In general, we assessed that we can fit subclones and tails for a wide range of  
805 parameter values, but overlapping distributions complicate the inference. MOBSTER does not show biases and  
806 can identify subclones, even when they have low VAF (Supplementary Note).

807

808 From multi-region data (Supplementary Note) of polyclonal tumors we identified three confounders that inflate  
809 the number of clones reported by a “standard” analysis. The confounders contribute Binomial clusters that  
810 cannot be directly linked to clonal evolution patterns originating from positive selection. Branching structures  
811 originating from the confounders are also misleading, and do not reflect selection-driven branched evolution.  
812 One of the confounders can be solved by MOBSTER; two require extra heuristics discussed in the Supplementary  
813 Note.

814

## 815 Analysis of patient derived data

816

817 The description of all the data analyzed is in the Supplementary Note, as well as in the Supplementary Data. All  
818 summary statistics for all fit samples of this paper are available in Supplementary Table 1.

819

## 820 Data Availability

821

822 Data in Figure 3a were from Nik-Zainal *et al.* 2012<sup>3</sup>. Data in Figure 3b were from Griffith *et al.* 2015<sup>20</sup>. Data in  
823 Figure 3c-e were cases from Cross *et al.* 2018<sup>21</sup>, here re-sequenced at higher sequencing depth. Sequence data  
824 from those colorectal cancer cases have been deposited at the European Genome-phenome Archive (EGA),  
825 which is hosted by the EBI and the CRG, under accession number EGAS00001003066. Further information  
826 about EGA can be found on <https://ega-archive.org>. Diploid SNVs and copy number calls are available in the  
827 Supplementary Data in vignette “5. Multi-region cross-sectional colorectal carcinomas”. Data in Figure 3f were  
828 from Lee *et al.* 2019<sup>24</sup>. Data in Figure 4 are available through the PCAWG consortium<sup>25</sup>. Whole-genome variant  
829 call data in Figure 5 that were not available from the original publication, were provided upon email request by  
830 Korber *et al.* 2019<sup>28</sup>.

831

## 832 Code Availability

833

834 MOBSTER is available as an R package at <https://github.com/sottorivalab/mobster/>; future updates, as well as  
835 all vignettes and manuals are maintained at <https://caravagn.github.io/mobster/>. A repository with all  
836 Supplementary Data is available at [https://github.com/sottorivalab/mobster\\_supp\\_data](https://github.com/sottorivalab/mobster_supp_data). Supplementary Data  
837 contain vignettes that show the analysis of single-sample and multi-region simulated tumors, the whole analysis  
838 of multi-region colorectal samples and single-sample lung cancers, and summary results from the PCAWG and  
839 GBM cohorts. Somatic single nucleotide variants and copy number calls used for the analysis of multi-region

840 colorectal samples are also available as Supplementary Data. The implementation of all other R packages that  
841 we have developed are available at <https://caravagn.github.io/>.

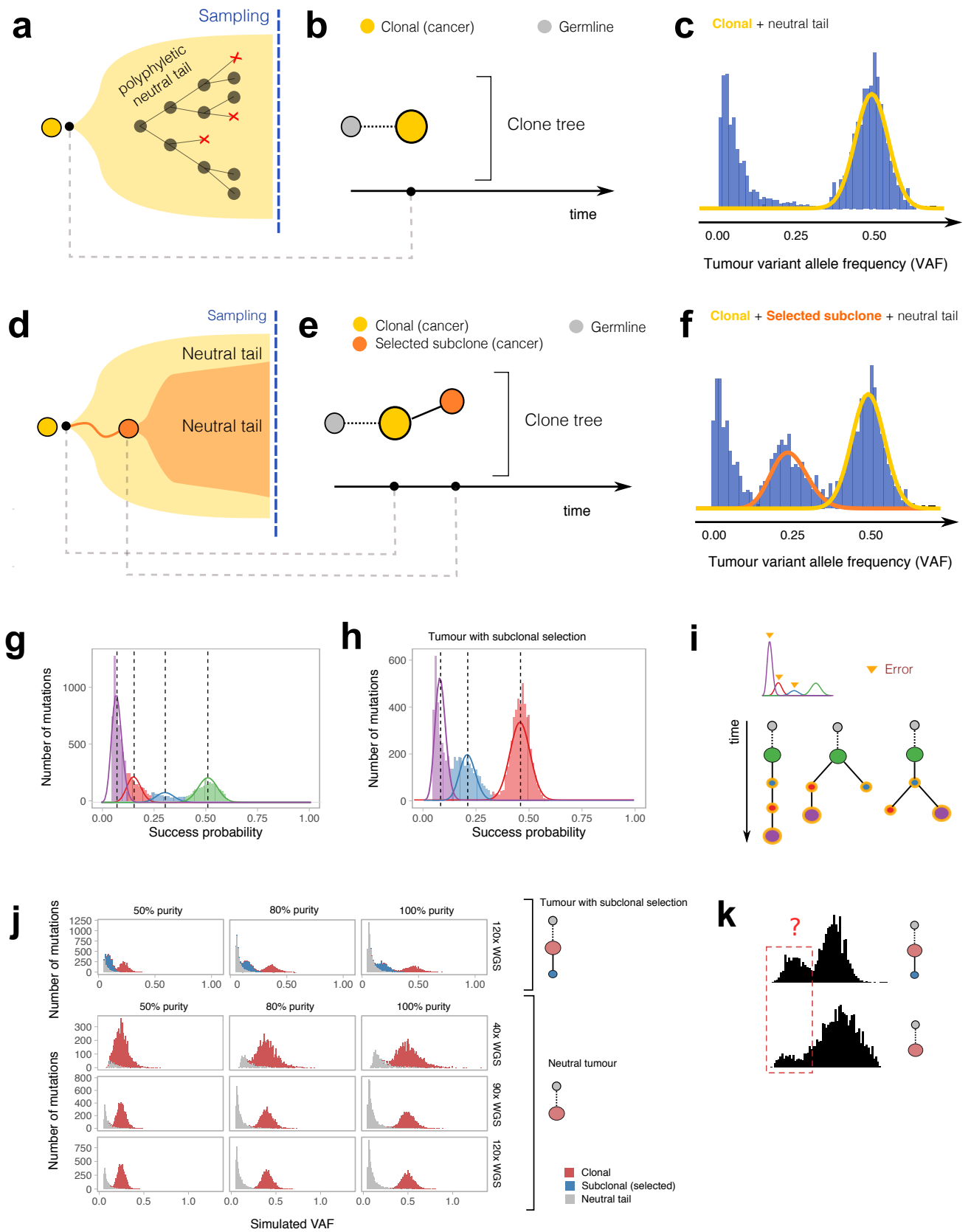
842

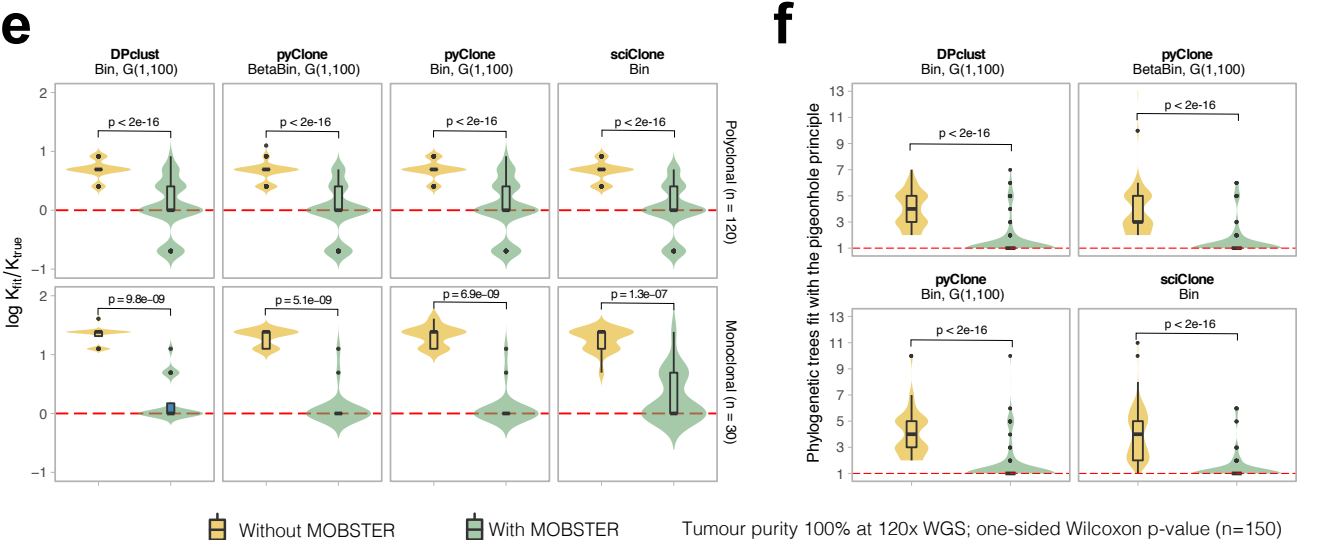
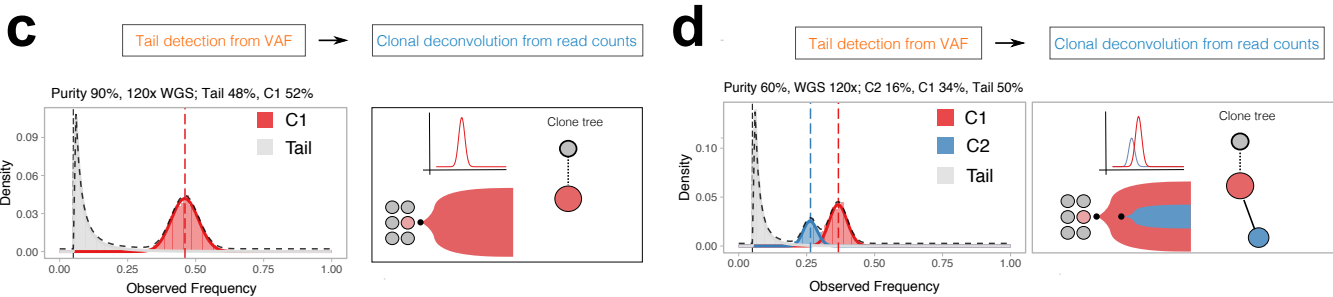
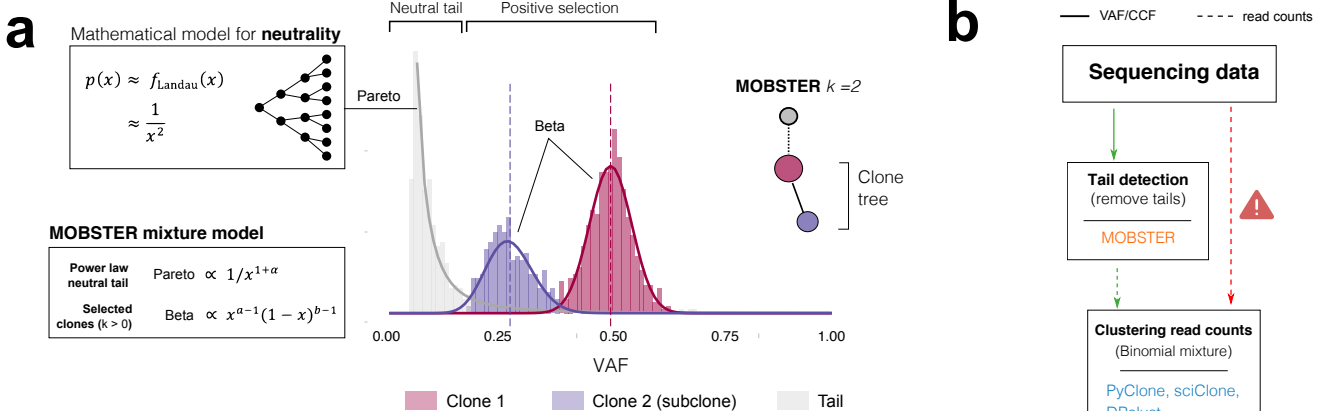
## 843 Methods-only References

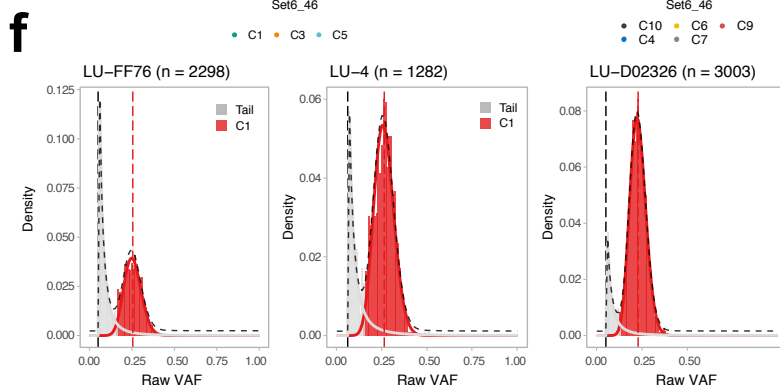
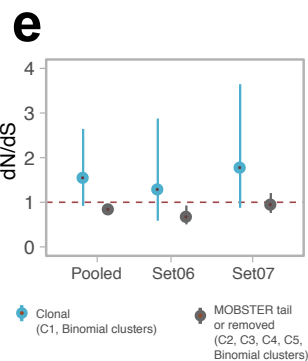
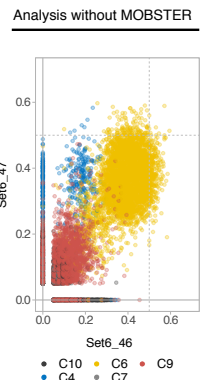
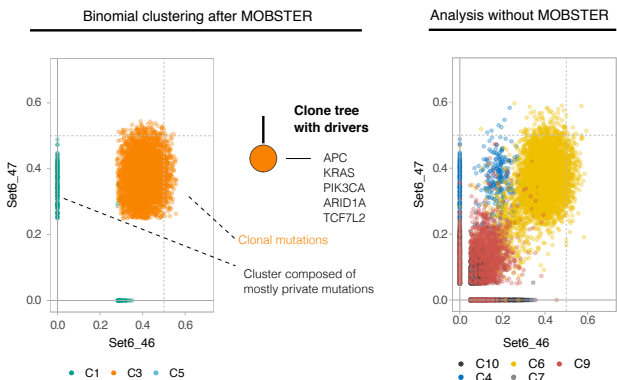
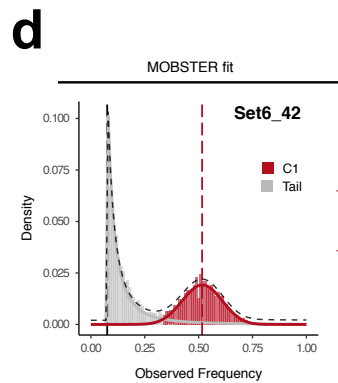
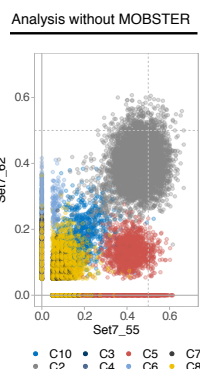
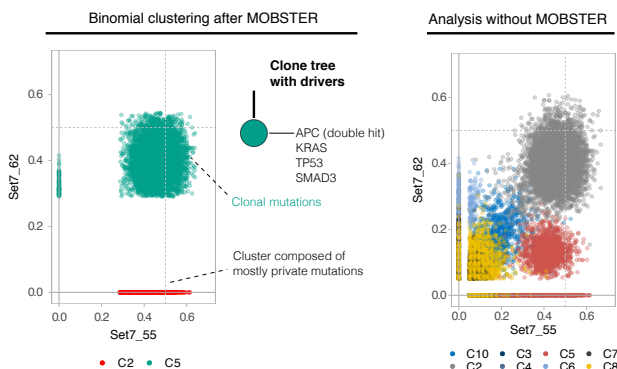
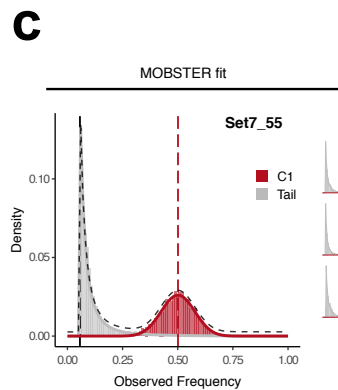
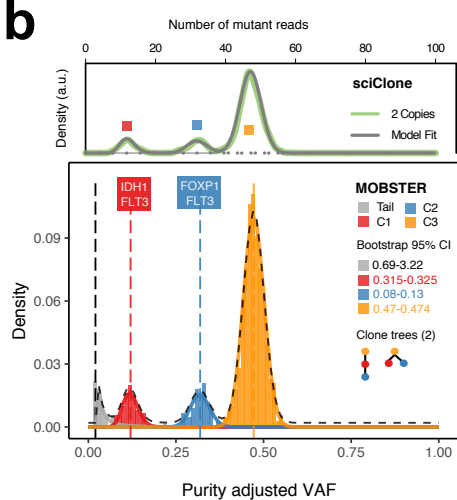
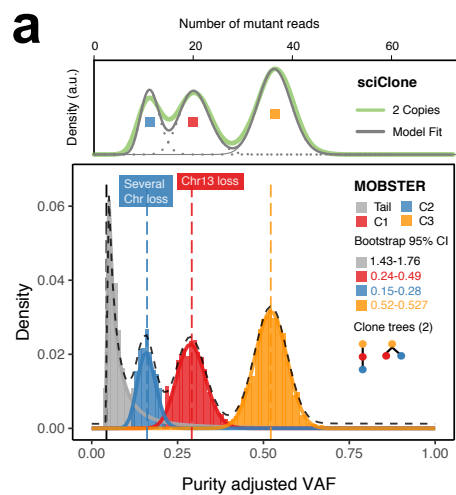
844

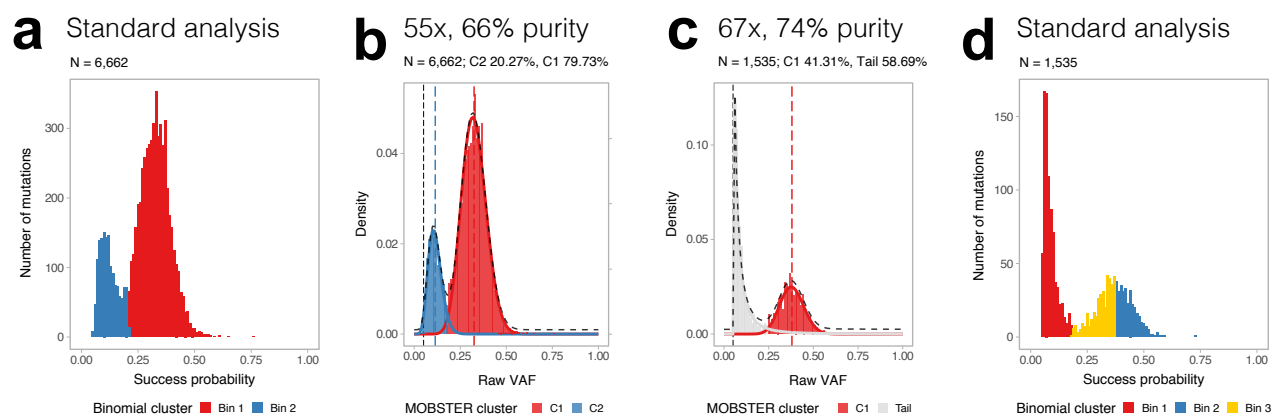
- 845 42. Fusco, D., Gralka, M., Kayser, J., Anderson, A. & Hallatschek, O. Excess of  
846 mutational jackpot events in expanding populations revealed by spatial Luria–  
847 Delbrück experiments. *Nat Comms* **7**, 12760 (2016).
- 848 43. Teh, Y. W. in *Encyclopedia of Machine Learning* 280–287 (Springer, Boston, MA,  
849 2011).
- 850 44. Ghahramani, Z., Jordan, M. I. & Adams, R. P. Tree-Structured Stick Breaking for  
851 Hierarchical Data. 19–27 (2010).
- 852 45. Ma, Z. & Leijon, A. Bayesian Estimation of Beta Mixture Models with Variational  
853 Inference. *IEEE Transactions on Pattern Analysis and Machine Intelligence* **33**, 2160–  
854 2173 (2011).
- 855 46. Clauset, A., Shalizi, C. R. & Newman, M. E. J. Power-Law Distributions in Empirical  
856 Data. *SIAM Review* **51**, 661–703 (2009).
- 857 47. Schröder, C. & Rahmann, S. A hybrid parameter estimation algorithm for beta  
858 mixtures and applications to methylation state classification. *Algorithms for Molecular*  
859 *Biology* 2017 12:1 **12**, 21 (2017).
- 860 48. Biernacki, C., Celeux, G. & Govaert, G. Assessing a mixture model for clustering with  
861 the integrated completed likelihood. *IEEE Transactions on Pattern Analysis and*  
862 *Machine Intelligence* **22**, 719–725 (2000).
- 863



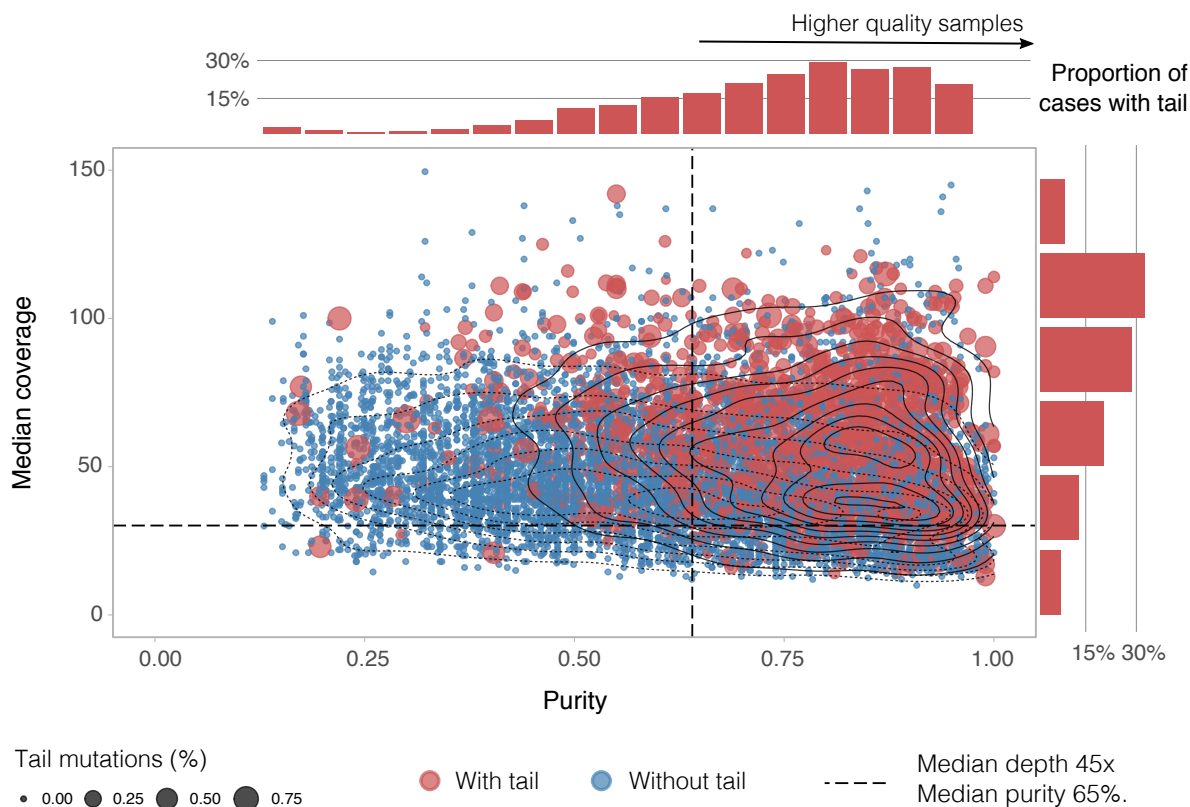




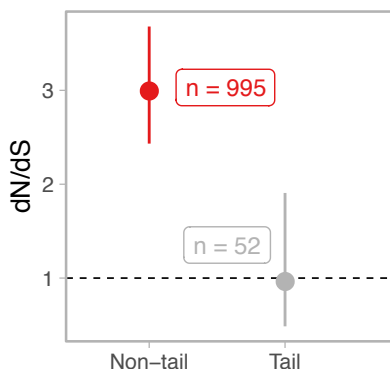




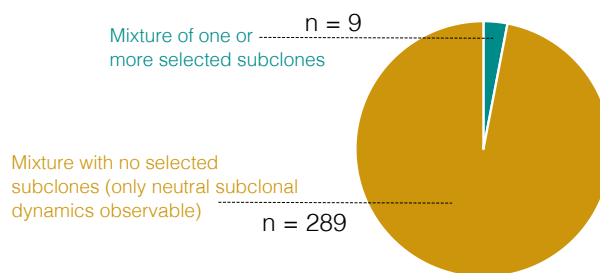
**e** Estimated neutral tails in PCAWG (n = 2,566 samples, 8,655 fits by karyotypes)

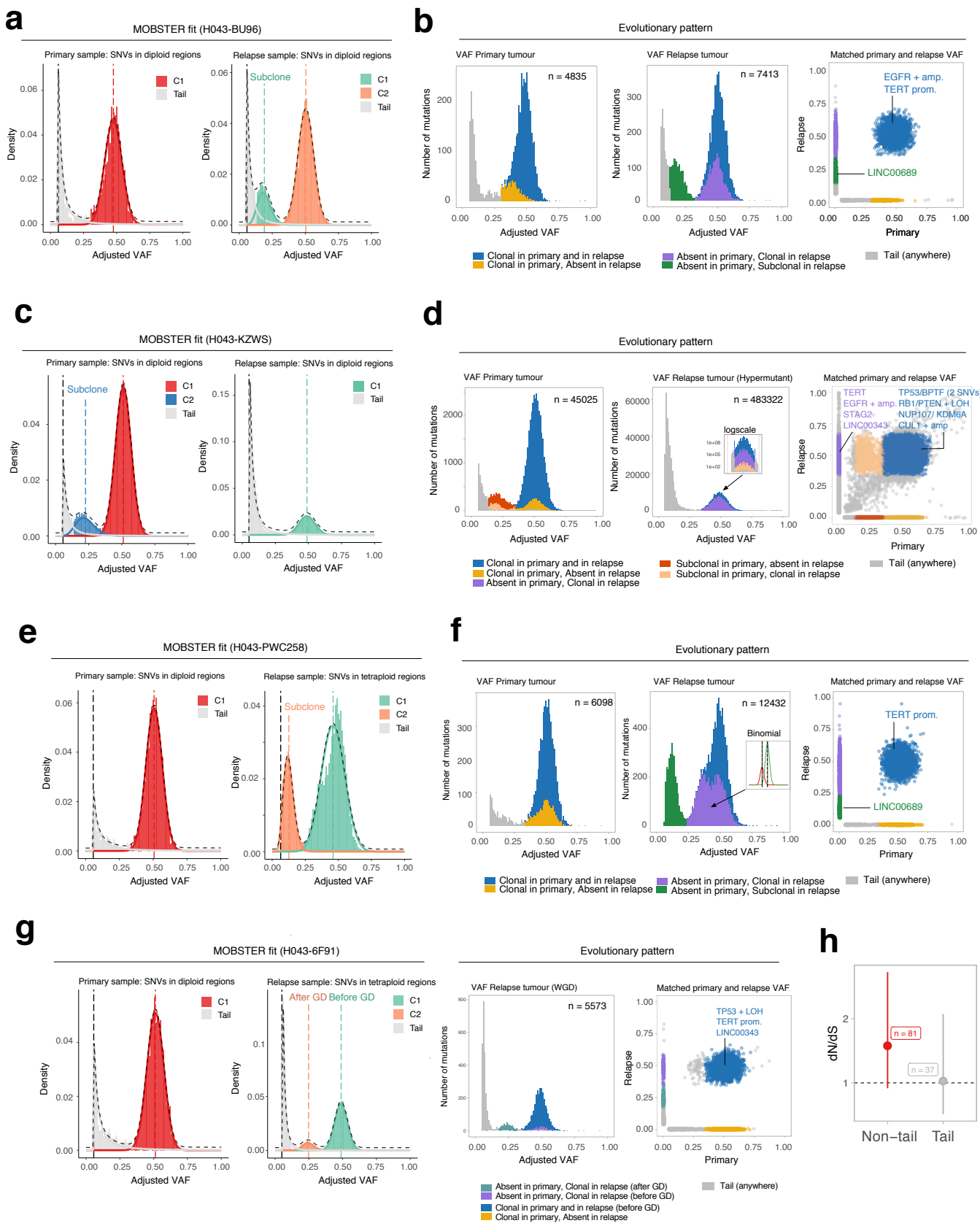


**f** 191 curated pan-cancer driver genes



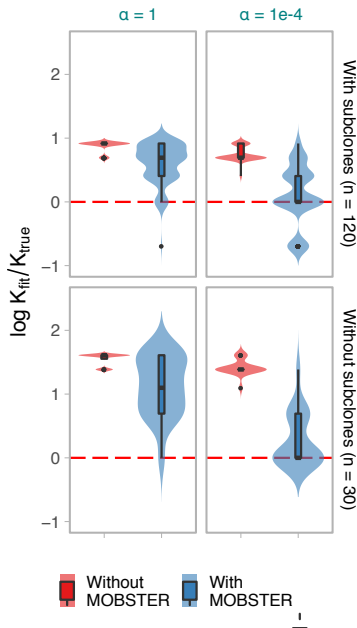
**g** Binomial clusters from non-tail mutations



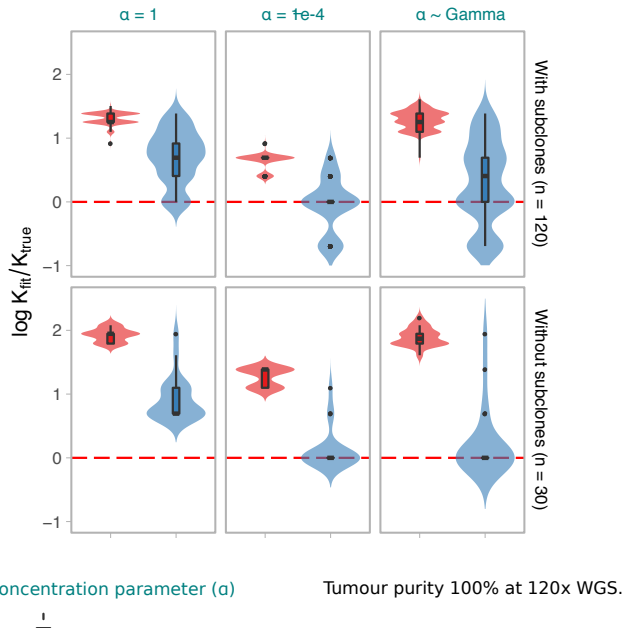


**a****Dirichlet mixtures**

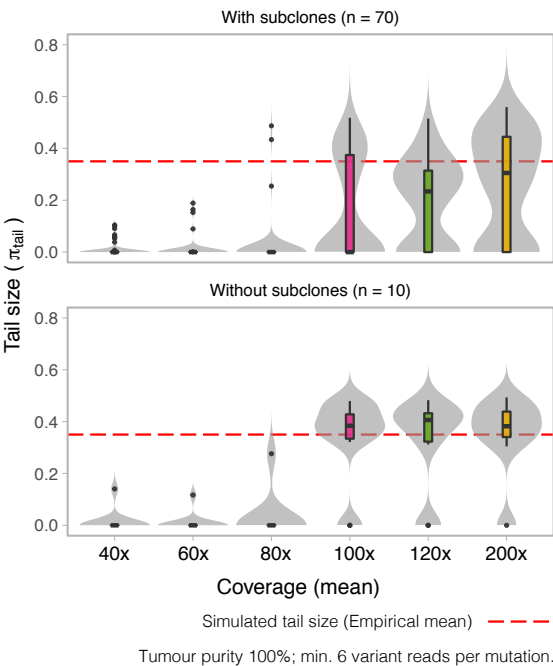
Variational fit (n = 150)

**b****Dirichlet Process**

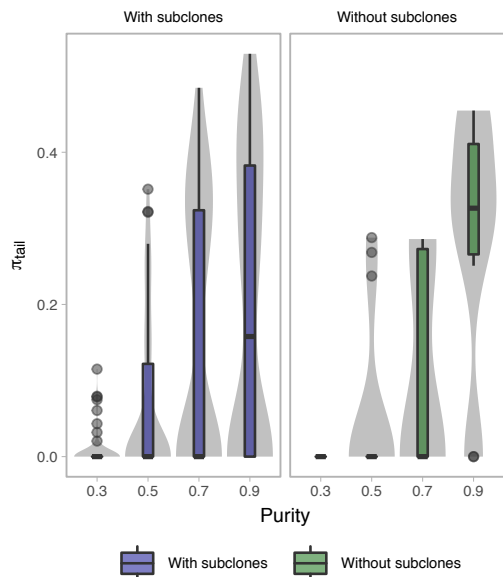
10,000 MCMC steps per chain (n = 150)

**c****Tail size with different coverage (n = 480)**

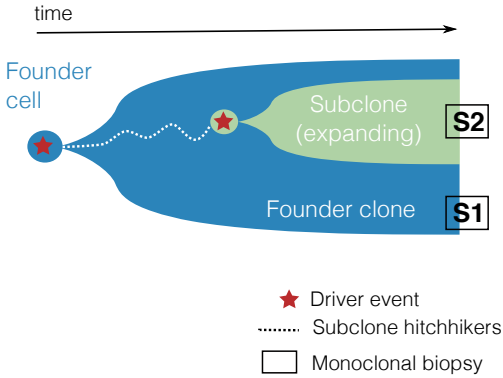
MOBSTER fit with ICL (n = 80 x 6)

**d****Tail's size with different purity (n = 320)**

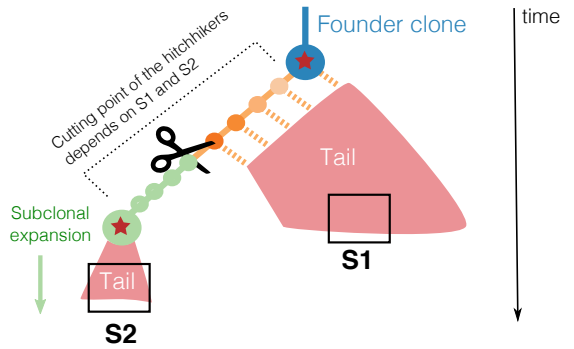
MOBSTER fit with ICL (n = 80 x 4)



### a Muller plot of a polyclonal tumour

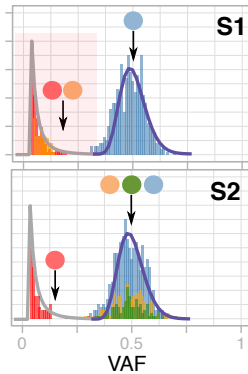


### b Phylogenetic tree (sketch)



### c Expected data distribution of VAF values (cartoon)

Hitchhikers frequency	
Subclone	Rest of the tumour
100%	~50%
100%	~25%
100%	~12.5%
100%	~6.25%
100%	0%



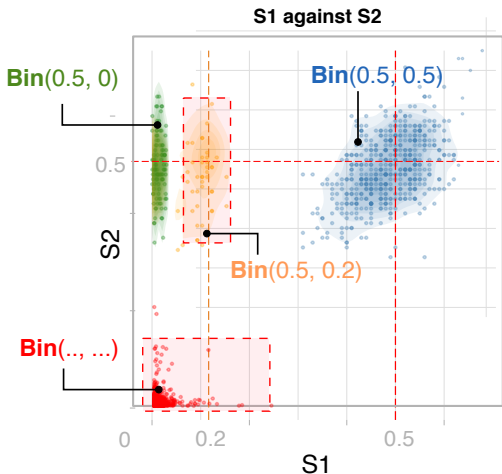
Cells **without** the subclonal driver



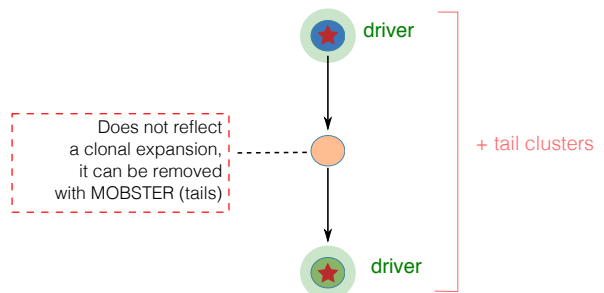
Cells **with** the subclonal driver



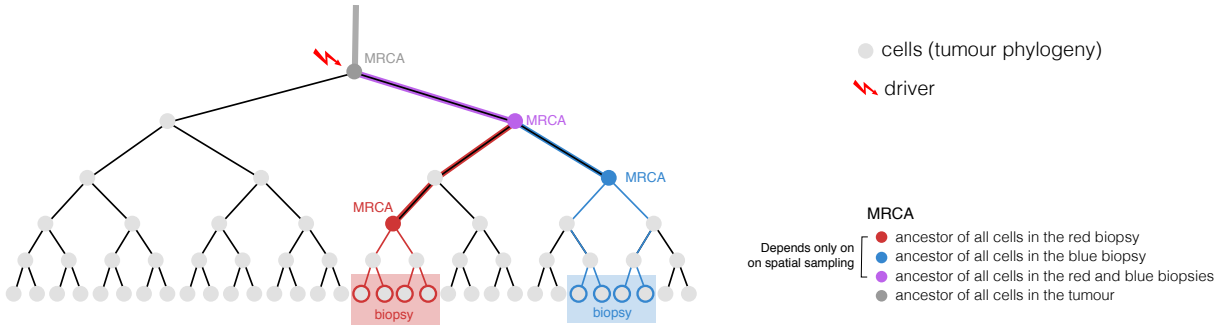
Binomial clusters (standard analysis)



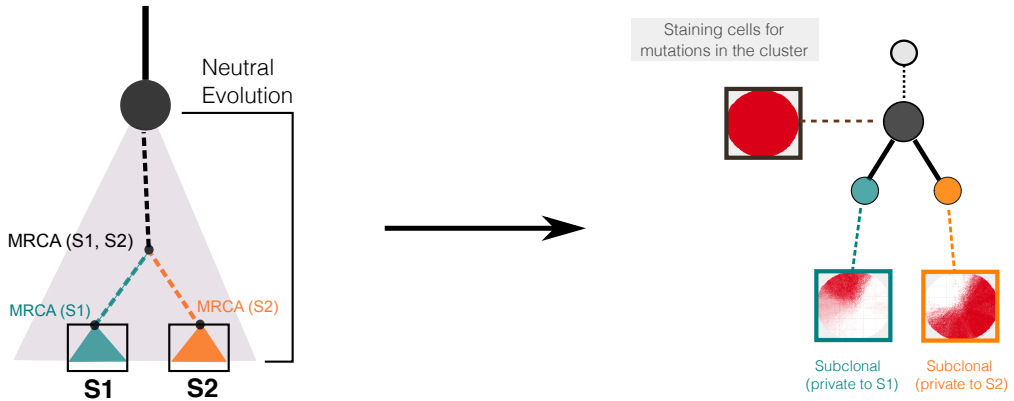
### Hitchhiker mirage



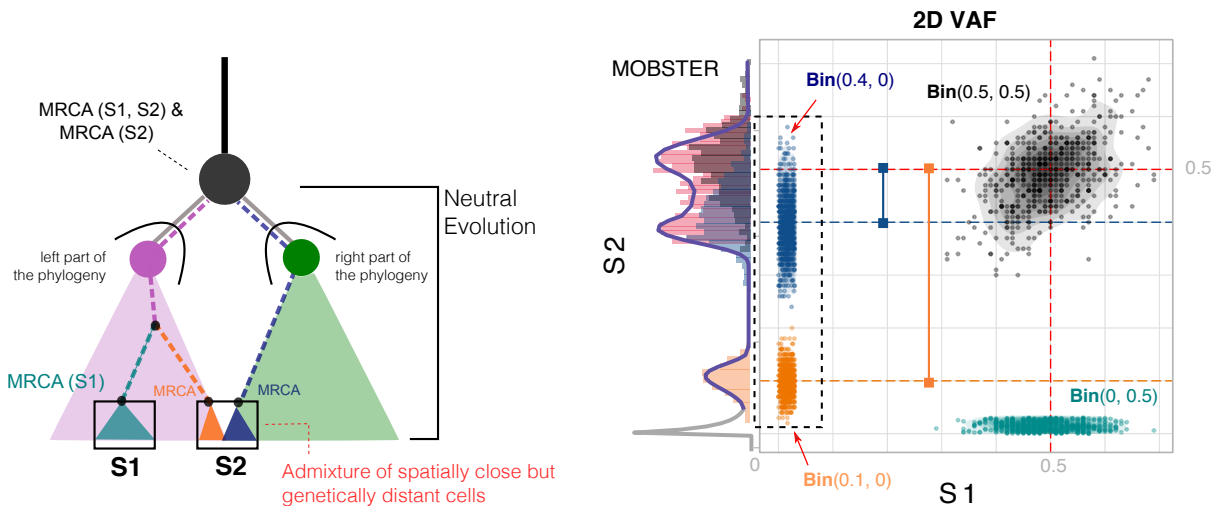
## a Example of Most Recent Common Ancestor (MRCA)



## b MRCA effect and virtual staining matching the clone tree

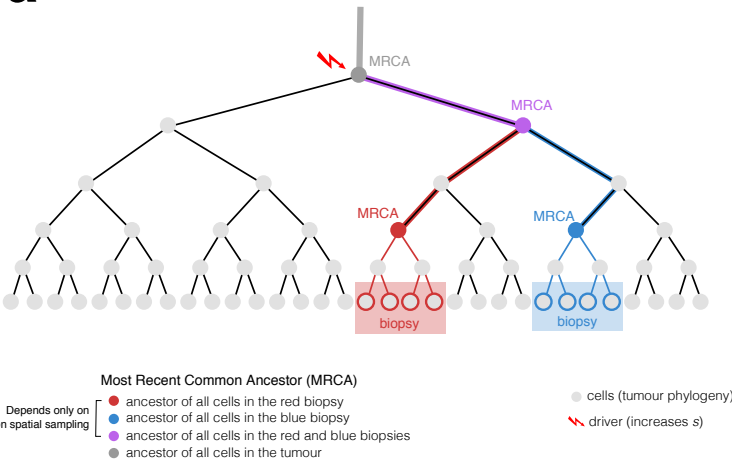


## c Admixing effect and expected data distribution of VAF values (cartoon)

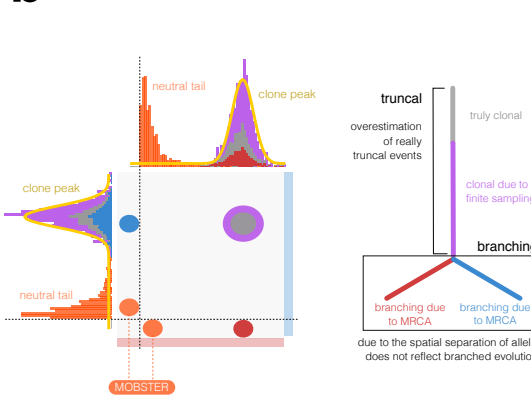




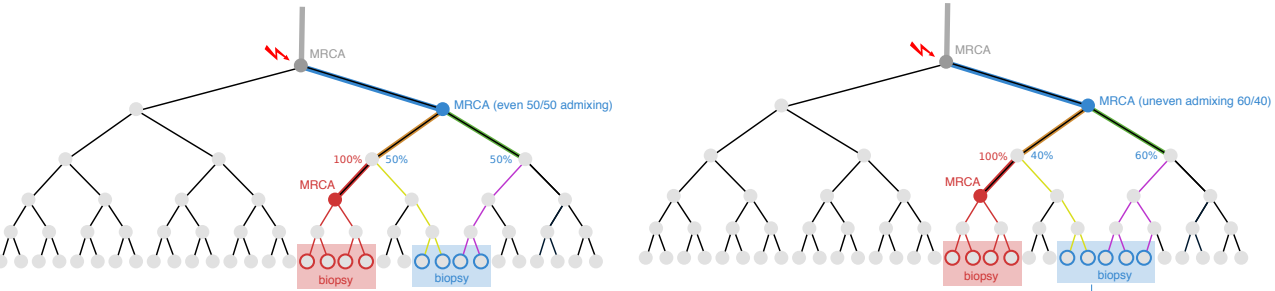
### a Spatial sampling ancestors that confound the inference



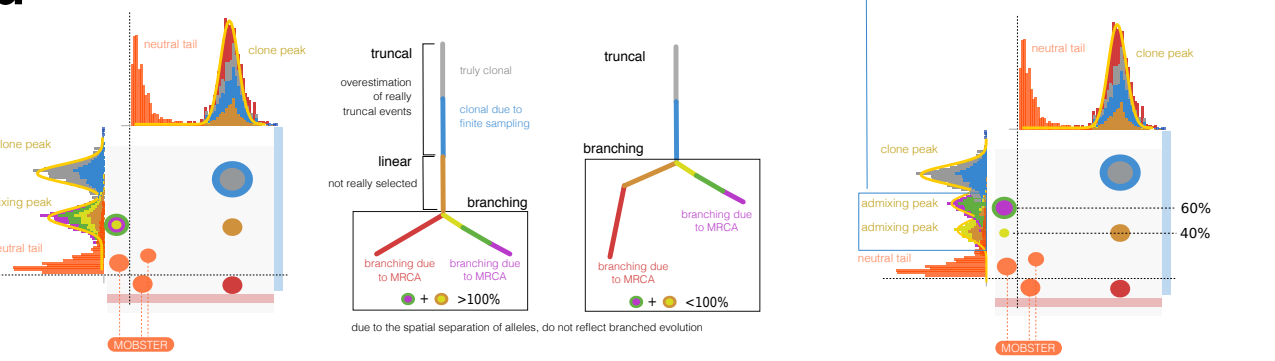
### b Data distribution and phylogenetic model



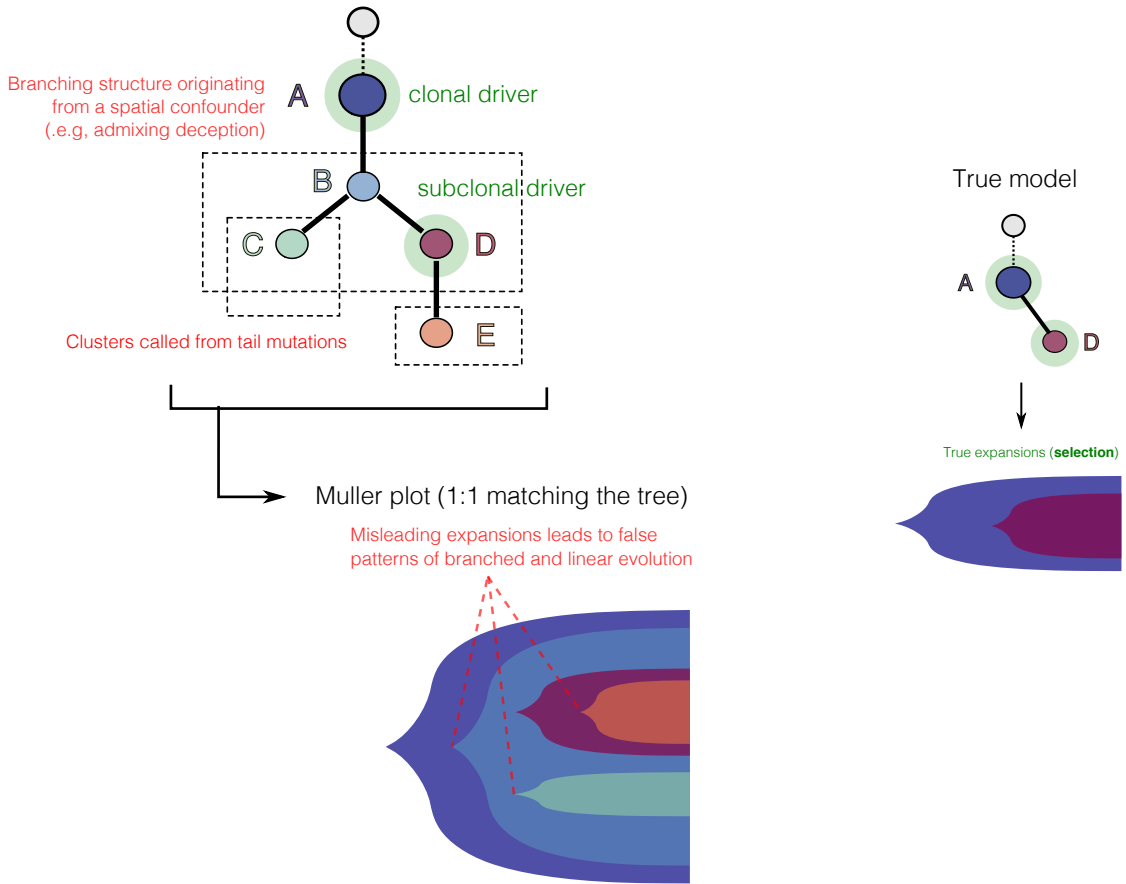
### c Spatial sampling admixed ancestors that confound the inference (in different proportions)



### d Data distributions and phylogenetic models



# a Turning a "standard" clone trees into a model of clonal evolution



# b True cell phylogeny (single-cell) that generates data consistent with the above tree

